



TITLE:

Rhodopsin-mediated light-off-induced protein kinase A activation in mouse rod photoreceptor cells

AUTHOR(S):

Sato, Shinya; Yamashita, Takahiro; Matsuda, Michiyuki

CITATION:

Sato, Shinya ...[et al]. Rhodopsin-mediated light-off-induced protein kinase A activation in mouse rod photoreceptor cells. *Proceedings of the National Academy of Sciences of the United States of America* 2020, 117(43): 26996-27003

ISSUE DATE:

2020-10

URL:

<http://hdl.handle.net/2433/264443>

RIGHT:

This is a postprint of the article, which has been published in final form at <https://doi.org/10.1073/pnas.2009164117>.; This is not the published version. Please cite only the published version. この論文は出版社版ではありません。引用の際には出版社版をご確認ください。

PNAS

www.pnas.org

1

2 Main Manuscript for

3 **Rhodopsin-mediated Light-off-induced Protein Kinase A Activation in**
4 **Mouse Rod Photoreceptor Cells.**

5 Shinya Sato^{a*}, Takahiro Yamashita^b, and Michiyuki Matsuda^{a,c}

6 ^aLaboratory of Bioimaging and Cell Signaling, Graduate School of Biostudies, Kyoto University, Kyoto
7 606-8501 Japan;

8 ^bDepartment of Biophysics, Graduate School of Science, Kyoto University, Kyoto 606-8502, Japan;

9 ^cDepartment of Pathology and Biology of Diseases, Graduate School of Medicine, Kyoto University, Kyoto
10 606-8501 Japan;

11 *To whom correspondence should be addressed: Shinya Sato

12 **Address:** Laboratory of Bioimaging and Cell Signaling, Graduate School of Biostudies, Kyoto University,
13 Kyoto 606-8501 Japan;

14 **TEL:** +81-75-753-9450

15

16 **Email:** sato.shinya.7e@kyoto-u.ac.jp

17 ORCIDs: Shinya Sato, 0000-0002-5978-0975; Takahiro Yamashita, 0000-0002-7956-9288; Michiyuki
18 Matsuda, 0000-0002-5876-9969

19 Classification

20 BIOLOGICAL SCIENCES – Neuroscience

21 **Keywords**

22 Retina, Two-photon microscopy, FRET biosensor, Protein kinase A, Rhodopsin.

23 **Declaration of Competing Interests**

24 The authors declare no conflict of interest.

25 **Author Contributions**

26 S.S. and M.M. designed the research; S.S. performed the research; S.S. and T.Y. analyzed the data; and

27 S.S., T.Y. and M.M. wrote the paper.

28 **This PDF file includes:**

29 Main Text

30 Figures 1 to 6

31 **Abstract**

32 Light-induced extrasynaptic dopamine release in the retina reduces cAMP in rod
33 photoreceptor cells, which is thought to mediate light-dependent desensitization.
34 However, the fine time course of the cAMP dynamics in rods remains elusive due to
35 technical difficulty. Here, we visualized the spatio-temporal regulation of cAMP-
36 dependent protein kinase (PKA) in mouse rods by two-photon live imaging of retinal
37 explants of PKA^{chu} mice, which express a fluorescent biosensor for PKA. Unexpectedly,
38 in addition to the light-on-induced suppression, we observed prominent light-off-induced
39 PKA activation. This activation required photopic light intensity and was confined to the
40 illuminated rods. The estimated maximum spectral sensitivity of 489 nm and loss of the
41 light-off-induced PKA activation in rod-transducin-knockout retinas strongly suggest the
42 involvement of rhodopsin. In support of this notion, rhodopsin-deficient retinal explants
43 showed only the light-on-induced PKA suppression. Taken together, these results suggest
44 that, upon photopic light stimulation, rhodopsin and dopamine signals are integrated to
45 shape the light-off-induced cAMP production and following PKA activation. This may
46 support the dark-adaptation of rods.

47

48 **Significance Statement**

49 Rod photoreceptor cells mediate scotopic vision using rhodopsin and its downstream
50 signal transduction cascade to degrade cGMP. However, less is known about another rod
51 photoresponse: dopamine-mediated cAMP degradation. Cyclic AMP enhances the rod
52 photosensitivity, and therefore its degradation contributes to the visual desensitization.
53 Here, we show the fine time course of rod cAMP regulation using a two-photon
54 microscope and fluorescent protein probe for cAMP-dependent protein kinase (PKA).
55 Unexpectedly, the light-induced PKA suppression was followed by robust PKA
56 activation upon light-off. Our data strongly suggest the involvement of rhodopsin in this

57 activation, and thus the presence of its alternative output toward cAMP. The light-off-
58 induced PKA activation might contribute to an efficient dark-adaptation after the
59 transition from light to dark environment.
60

61 **Main Text**62 **Introduction**

63 Vertebrate photoreceptor cells, i.e., rods and cones, convert light information into
64 electrical signals through an enzymatic process called phototransduction (1-4). In this
65 process, light-activated visual pigments, rhodopsin in rods and cone visual pigments in
66 cones, activate heterotrimeric G-protein transducin and thereby phosphodiesterase,
67 culminating in the degradation of cyclic guanosine-3',5'-monophosphate (cGMP). The
68 reduction in cGMP concentration causes closure of cGMP-dependent channels in the
69 plasma membrane to evoke an electrical response. For the timely update of visual
70 information, activated visual pigments and their downstream enzymes are then rapidly
71 deactivated (5) and, when back in darkness, the cGMP level is restored by guanylate
72 cyclase (GC) (6, 7).

73 Ca^{2+} is the primary factor that decelerates the shut off processes of phototransduction
74 and thereby increases photoreceptor sensitivity (7-9). Under scotopic conditions, Ca^{2+}
75 flows into photoreceptor cells through the cGMP-gated cation channel. Ca^{2+} binds to
76 calcium-binding proteins, including S-modulin/recoverin and guanylate cyclase
77 activating proteins (GCAPs). Ca^{2+} -liganded S-modulin/recoverin inhibits rhodopsin
78 phosphorylation through inhibition of G protein coupled receptor kinase 1 (GRK1), to
79 delay the quenching of photoactivated rhodopsin by arrestin (10). On the other hand,
80 Ca^{2+} -liganded GCAPs are negatively modulated and do not activate the cGMP restoration
81 by GC (6). Thereby, high Ca^{2+} in scotopic conditions delays the recovery of the
82 photoresponse and increases the sensitivity of photoreceptor cells (5).

83 Recently, in addition to Ca^{2+} , cAMP has been suggested to increase photoreceptor
84 sensitivity (11). Similarly to the Ca^{2+} level, the cAMP level in photoreceptors is reduced
85 by light via a dopamine-mediated mechanism (12, 13). Dopamine is released
86 extrasynaptically from dopaminergic amacrine cells in a light-dependent manner (14, 15).

87 Photoreceptor cells detect dopamine with the dopamine receptor D4 (D4R) (16, 17),
88 which is coupled with G_i to inhibit adenylate cyclase (AC) and thereby to reduce cAMP
89 (18). A number of previous studies showed that cAMP-dependent protein kinase (PKA)
90 phosphorylates several phototransduction components. PKA phosphorylates GRK1 to
91 reduce its rhodopsin phosphorylation ability (19), regulator of G protein signaling 9-1 to
92 reduce its GTPase activating protein activity (20), phosducin to accelerate the trafficking
93 of transducin toward the outer segment (21), and GC to increase its sensitivity to Ca²⁺-
94 dependent inhibition (22). These studies suggest a role of PKA in increasing
95 photoreceptor sensitivity. Indeed, Astakhova and colleagues showed that
96 pharmacological activation of the cAMP production induces a two-fold increase in the
97 signal-to-noise ratio in frog rods (11, 23). Furthermore, PKA strengthens the electrical
98 coupling of photoreceptor cells via the phosphorylation of connexin36 (24) to increase
99 the visual sensitivity (25). Taken together, these findings strongly suggest that light
100 reduces cAMP levels to desensitize photoreceptor cells via PKA suppression. However,
101 unlike in the case of cGMP regulation, which has been studied electrophysiologically
102 with single-cell resolution and millisecond precision, there are currently no available
103 methods to monitor cAMP in living photoreceptor cells, which limits the systematic
104 characterization of its spatio-temporal regulation in photoreceptors.

105 Here, we used a new two-photon PKA activity imaging method to address this
106 deficiency. A retinal explant culture for imaging was prepared from PKAchu mice (26-
107 28) that ubiquitously express a Förster resonance energy transfer (FRET)-based PKA
108 activity sensor protein, AKAR3EV (29, 30). Unexpectedly, in addition to the
109 aforementioned light-on-induced PKA suppression, we observed a prominent light-off-
110 induced PKA activation in photoreceptor cells. This PKA activation was induced by
111 photopic light stimulation and confined to rod photoreceptor cells in the illuminated area.
112 Spectral sensitivity data suggested the involvement of rhodopsin in the PKA activation.

113 Consistent with this suggestion, the activation was not detected from retinal explants that
114 were deficient in rhodopsin signaling. Interestingly, the rhodopsin-deficient retinas
115 showed only light-on-induced PKA suppression. From these results, we propose that
116 rhodopsin and dopamine signals are integrated to shape the light-off-induced PKA
117 activation in rods.

118 Results

119 Ex vivo two-photon imaging delineates various layers of the PKAchu mouse retina.

120 First, we set up two-photon live imaging of the isolated mouse retina (Fig. 1A). A retina
 121 from a PKAchu mouse was flat-mounted on a culture insert. The insert was then placed
 122 under a two-photon microscope and perfused with oxygenated culture medium. The PKA
 123 biosensor AKAR3EV (SI Appendix, Fig. S1A) was expressed ubiquitously in PKAchu
 124 mice, which allowed us to delineate tissue morphology at the subcellular level in six
 125 different layers of the retina (Fig. 1 B-H, SI Appendix, Movie S1). The nuclear-sparing
 126 pattern was caused by the cytoplasmic localization of AKAR3EV (30). The outer nuclear
 127 layer (ONL) thickness at 1.0 mm superior from the optic nerve head (ONH) was $54.3 \pm$
 128 $2.9 \mu\text{m}$ (mean \pm SD, $n = 12$ retinas), which is comparable to the value for the young-adult
 129 wild-type (31). Intriguingly, a subset of cells in the photoreceptor layer (Fig. 1 E-H)
 130 expressed AKAR3EV much more abundantly (AKAR3EV^{high} cells) than the rest
 131 (AKAR3EV^{low} cells). Therefore, to prevent saturation of the detector, we needed to
 132 reduce the excitation laser power from the outer plexiform layer (OPL; arrow in Fig. 1H).
 133 Please note that this intensity difference does not mean high and low PKA activities.
 134 Although PKA increases the FRET efficiency of AKAR3EV (SI Appendix, Fig. S1A) to
 135 induce the spectral shift of the fluorescence, the corresponding intensity change is limited
 136 (SI Appendix, Fig. S1B).

137 In the OPL, the large size and shape of the AKAR3EV^{high} photoreceptor cells closely
 138 resembled the cone pedicles (Fig. 1E) (32). Moreover, the nuclei of the AKAR3EV^{high}
 139 photoreceptor cells (white arrowheads in Fig. 1H) were located near the interface
 140 between the ONL and photoreceptor segments layer (PRS). These observations strongly
 141 suggested that the AKAR3EV^{high} and AKAR3EV^{low} cells are cones and rods,
 142 respectively. This was confirmed by using rhodamine labeled peanut agglutinin (PNA-
 143 rhodamine), which specifically binds to the extracellular sheath of cones (33). As

144 expected, PNA-rhodamine labeled the tips of the AKAR3EV^{high} cells (Fig. 1I, SI
 145 Appendix, Movie S2). In conclusion, our two-photon imaging method clearly delineates
 146 the layer structure of the PKAchu retina and enables comparison of PKA activities in
 147 rods and cones.

148

149 **The PKAchu retina visualizes cell type-specific PKA regulation by dopamine.**

150 To confirm whether AKAR3EV detects PKA activity in the retina, we first examined the
 151 response to forskolin, which increases the cAMP level by stimulating AC. The mode of
 152 action of AKAR3EV and the method to generate PKA activity images were described
 153 previously (34, 35). Briefly, the signal intensity in the FRET-acceptor channel (FRET
 154 Ch) was divided by that of FRET-donor channel (CFP Ch) to obtain FRET/CFP
 155 pseudocolor images, which depict PKA activity (SI Appendix, Fig. S1B). As expected, 20
 156 μ M forskolin strongly increased FRET/CFP in all layers of the retina (SI Appendix, Fig.
 157 S2 A and B, Movie S3). Interestingly, this elevation was less pronounced in cones (white
 158 arrowheads in SI Appendix, Fig. S2A) than in rods, which may be ascribable to the
 159 difference in AC subtypes (36).

160 Next, we examined the response to dopamine, which is one of the major
 161 neurotransmitters that modulates visual processing in the retina (37). Dopamine either
 162 activates or inactivates PKA, depending on the type of dopamine receptors: D1-like
 163 receptors (D1R and D5R) activate PKA via G_s , whereas D2-like receptors (D2R, D3R
 164 and D4R) suppress PKA via G_i (13). In the mouse retina, D1R is expressed in horizontal
 165 cells and a subset of bipolar and amacrine cells in the inner retina (38). On the other hand,
 166 D4R is expressed in photoreceptor cells (16, 24). In agreement with this layer-specific
 167 distribution, 10 μ M dopamine increased FRET/CFP values in the inner plexiform and
 168 inner nuclear layers, and decreased them in photoreceptor cells (SI Appendix, Fig. S2 C

169 and *D*, Movie S4). Therefore, we concluded that AKAR3EV in the PKAchu retina
 170 detects both PKA activation and suppression.

171

172 **Light-induced PKA suppression is followed by an unexpected “overshoot” of**
 173 **activation in photoreceptor cells.**

174 According to previous studies, light induces extrasynaptic dopamine release from
 175 dopaminergic amacrine cells, which reduces cAMP in photoreceptor cells (16, 39, 40).
 176 However, previous studies did not elucidate the fine time course of this response;
 177 therefore, we time-lapse imaged the light-induced cAMP reduction via PKA activity
 178 change. Dark- and light-adapted PKAchu retinas were prepared for imaging (please see
 179 *SI Appendix, Supplementary Methods* for details about preparations). As expected from
 180 previous studies that reported the elevated photoreceptor cAMP level in darkness (40,
 181 41), the basal PKA activity in photoreceptor cells was significantly greater in the dark-
 182 adapted retina (Fig. 2 *A* and *B*, PRS). To measure the time course of the photoresponse, a
 183 stimulation light was delivered onto the retina (*SI Appendix, Supplementary Methods*).
 184 Upon a brief 6 sec light stimulation, photoreceptors in the dark-adapted retina showed a
 185 large drop in PKA activity (Fig. 2*C* and *D*, dark). Unexpectedly, however, PKA activity
 186 rebounded over the basal level, and the increased activity level continued for 30 min. On
 187 the other hand, photoreceptors in the light-adapted retina exhibited only a modest
 188 suppression of PKA (Fig. 2*C* and *D*, light), but showed marked PKA activation for 15
 189 min. The suppression was detected within 12 sec from the stimulation, and subsequent
 190 activation was detected at 50 ± 5 sec and peaked at 214 ± 16 sec (mean \pm SD, $n = 5$; Fig.
 191 2*E*).

192 In an effort to visualize the light-induced suppression more clearly, we applied a
 193 longer 10 min stimulation to the light-adapted retina (Fig. 2 *F* and *G*, *SI Appendix*,
 194 Movie S5). In this case, photoreceptor PKA activity exhibited a transient drop in the first

195 2 min, but returned to the basal level for the remaining 8 min. Then, to our surprise, PKA
 196 was prominently activated upon light-off. We speculate that, upon the light-on, the
 197 dopamine-mediated PKA suppression occurred and was observed as a transient drop at 2
 198 min. But simultaneously, an antagonizing light-induced PKA activation occurred with
 199 slow kinetics that canceled out the suppression during the subsequent 8 min. Then, upon
 200 light-off, the dopamine effect was removed instantly probably due to an efficient
 201 dopamine clearance from the extrasynaptic space (42), and only the activation remained
 202 to shape the apparent off response. Because such light-induced PKA activation has not
 203 been reported in normal photoreceptor cells [but see (43, 44)], hereafter, we focused on
 204 this PKA activation using light-adapted retinas.

205

206 **Light-off-induced PKA activation occurs exclusively in rod photoreceptor cells.**

207 To determine cell type specificity of the light-off-induced PKA activation, we first
 208 examined spatial confinement of the activation in photoreceptor cells. The light spot was
 209 projected at the center of the view field (dashed circle in Fig. 3A), and time courses of the
 210 PKA activation were compared among four areas: three inside and one outside of the
 211 light spot (Fig. 3B). The activation was sharply confined to the illuminated area (Fig. 3C).

212 We also confirmed that the response was mediated by the phosphorylation on the
 213 FRET biosensor AKAR3EV, but not by bleaching/switching of its fluorophores.
 214 PKAchu-NC mice were used for this purpose. This negative control mouse strain carries
 215 AKAR3EV-NC, which has an alanine substitution at the threonine residue in the PKA
 216 substrate motif (SI Appendix, Fig. S1C) (29). In PKAchu-NC retinas, light-induced
 217 changes were not observed (Fig. 3 A and C, SI Appendix, Movie S6), confirming that the
 218 light response in the PKAchu retina is induced by the phosphorylation of the AKAR3EV.

219 Next, to study the cell-type specificity of the PKA activation, we performed 5D
 220 imaging (x, y, z, time and PKA activity). Longitudinal reconstruction images showed that

221 PKA was activated exclusively in photoreceptor cells, especially at PRS (Fig. 3 *D* and *E*,
 222 SI Appendix, Movie S7). A small number of cells in PRS showed less activation (Fig.
 223 3*D*, arrowheads) than did surrounding cells, suggesting that PKA was activated less
 224 efficiently in cones than in rods. Indeed, rod-specific PKA activation was visualized in
 225 high-magnification cross-sectional images (Fig. 3 *F* and *G*, SI Appendix, Movie S8).
 226 Taken together, these results indicated that the light-off-induced PKA activation occurs
 227 exclusively in light-exposed rod photoreceptor cells. In the following experiments, we
 228 further characterized this PKA activation in rods.

229

230 **Light-induced PKA activation is driven by rhodopsin and transducin.**

231 To identify the photopigment that drives the light-off-induced PKA activation, we
 232 analyzed the spectral sensitivity of the response. For this purpose, responses toward
 233 various intensities of light were recorded from rods (SI Appendix, Fig. S3*A*).
 234 Measurements were performed for seven different wavelengths to obtain a series of
 235 intensity-response relationships (SI Appendix, Fig. S3*B*). Then, half-saturating light
 236 intensities ($I_{1/2}$) were estimated by fitting. The inverse of $I_{1/2}$ values were plotted as a
 237 function of wavelength to obtain the spectral sensitivity (Fig. 4*A*). Assuming that the
 238 light-induced PKA activation would be triggered by an opsin-family photopigment, the
 239 data was fitted with an A1-pigment spectral template (45). The estimated λ_{\max} was 489
 240 nm, which suggests the involvement of rhodopsin (500 nm), isorhodopsin (487 nm) (46),
 241 and M-cone pigment (508 nm) in the PKA activation. Intriguingly, the estimated
 242 maximum amplitude increased as the wavelength became longer (SI Appendix, Fig.
 243 S3*C*), which is opposite to the activity regulation of melanopsin (see Discussion for
 244 detail).

245 To validate the involvement of rhodopsin in the light-off-induced PKA activation, we
 246 crossed PKA^{chu} mice with *Gnat1*^{-/-} mice, which lack the α subunit of the G-protein

247 transducin and are deficient in rhodopsin-mediated signal transduction in rods (47). The
 248 amplitude of the response in PRS was clearly decreased in PKAchu *Gnat1*^{+/-} and
 249 completely lost in PKAchu *Gnat1*^{-/-} (Fig. 4B), showing the critical roles of rhodopsin and
 250 transducin in the light-off-induced PKA activation. Notably, the estimated half-saturating
 251 light intensity for 500 nm light was 6.5×10^7 photons μm^{-2} (SI Appendix, Fig. S3B),
 252 which is $>10^4$ -fold greater than that of the visual photoresponse in rods (48). In such a
 253 high intensity range, the normal rod phototransduction is completely saturated. Thus,
 254 these data suggest the presence of an alternative rod phototransduction mechanism, which
 255 is activated exclusively with intense illumination.

256

257 **Both rhodopsin and isorhodopsin were detected in our light-adapted retinal explant.**

258 The estimated λ_{max} of the light-off-induced PKA photoresponse (489 nm) was 11 nm
 259 shorter than the absorption maximum of rhodopsin (500 nm). To study the cause of this
 260 blue-shift, we analyzed the absorption spectrum of photopigment extracted from our
 261 light-adapted retinal explant. Wild-type C57BL6/J (B6J) retinas were flat-mounted using
 262 the protocol performed in the PKA activity imaging, then, solubilized for absorption
 263 measurements. As a control, retinas from dark-adapted mice were collected under dim
 264 red light. Absorption of photopigment was detected from both light- and dark-adapted
 265 retinas at around 500 nm (Fig. 5A). The peak height of the light-adapted sample was $16 \pm$
 266 1% (mean \pm SD, $n = 3$) of the height observed for the dark-adapted control. Surprisingly,
 267 the absorption maximum of the light-adapted preparation was detected at 495 ± 2 nm
 268 (mean \pm SD, $n = 3$; Fig. 5B, Light), which was 7 nm shorter than that of the dark-adapted
 269 control (504 ± 1 nm; Fig. 5B, Dark) and well fitted with the spectral sensitivity plot of the
 270 light-off-induced PKA activation (Fig. 5C).

271 We speculated that the blue-shifted absorbance was caused by the formation of
 272 isorhodopsin, which contains 9-*cis* retinal and shows an absorption maximum at 487 nm

273 (46). Indeed, the obtained absorption spectrum was fitted well with the sum of the
 274 rhodopsin and isorhodopsin templates (Fig. 5D). To verify the presence of isorhodopsin,
 275 the chromophore composition was determined by normal phase high performance liquid
 276 chromatography (HPLC; Fig. 5E). Most of 11-*cis* retinal, which comprises $90 \pm 3\%$
 277 (mean \pm SD, $n=2$) of total retinoids in the dark-adapted control (Fig. 5 E and F, Dark),
 278 was converted to all-*trans* retinal and all-*trans* retinol in the light-adapted sample (Fig. 5
 279 E and F, Light). In agreement with the absorbance data, 11-*cis* retinal and 9-*cis* retinal
 280 were also detected at comparable levels: $9.0 \pm 2.3\%$ and $8.3 \pm 0.8\%$, respectively (mean \pm
 281 SD, $n = 3$; Fig. 5E and F, Light). Therefore, we concluded that isorhodopsin is formed
 282 specifically in the light-adapted retinal explants and produces the blue-shifted spectral
 283 sensitivity of the light-off-induced PKA activation.

284

285 **Rhodopsin-deficient albino PKAchu rods show only the light-on-induced PKA**
 286 **suppression.**

287 To further investigate the involvement of rhodopsin, we used albino mice, which show a
 288 greater reduction in rhodopsin level compared to their wild-type counterparts when kept
 289 under bright light (49). Although, rhodopsin content in the dark-adapted albino retina was
 290 $51 \pm 5\%$ (mean \pm SD, $n = 4$) to the wild-type level, surprisingly, that of the light-adapted
 291 albino retina was less than the detection limit (Fig. 6A, Albino), without any thinning in
 292 the ONL thickness ($53.9 \pm 1.3 \mu\text{m}$ at 1 mm superior from the ONH; mean \pm SD, $n = 6$
 293 retinas). The albino retina exhibited markedly higher basal PKA activity in the PRS layer
 294 than the wild-type (Fig. 6 B and C). This high basal PKA activity in PRS was suppressed
 295 to nearly the wild-type level in the presence of 100 nM exogenous dopamine (Fig. 6D),
 296 suggesting a decreased dopamine level in the albino retina. In fact, the albino mice used
 297 in this study (B6N-Tyr^{c-Brd}/BrdCrCrI; B6 albino) are deficient in tyrosinase, which
 298 supports dopamine biogenesis (50).

299 We performed the photostimulation experiments with albino PKAchu retinas. In stark
300 contrast to the wild-type, only transient suppression was observed following a brief 6 sec
301 stimulation (Fig. 6E, Albino). Moreover, the PKA activity was kept at a low level during
302 a 10 min stimulation and returned to the basal level upon light-off, without a prominent
303 overshoot (Fig. 6F, SI Appendix, Movie S9). These data further support the notion that
304 rhodopsin plays a critical role in the light-off-induced PKA activation in rods.

305 Discussion

306 In the present study, we report a two-photon live imaging method to visualize PKA
307 activity in all layers of the retina (Fig. 1, SI Appendix, Fig. S2, Movies S1-S4) and
308 describe the light-off-induced PKA activation in rods (Fig. 3, SI Appendix, Movies S7
309 and S8). The light-on-induced reduction of retinal cAMP was reported in previous studies
310 (16, 41, 51). Here, our live imaging approach with high spatiotemporal resolution has
311 succeeded in characterizing the light-off-induced PKA activation. Application of two-
312 photon microscopy to the retina is technically difficult because visual pigments are
313 substantially activated by both high-power infrared excitation laser and fluorescence
314 emission from probes, which cause a low-photopic level of activation in the visual
315 transduction system (52) (*SI Appendix, Supplementary Text*). The light-off-induced PKA
316 activation was readily observed, probably because this response requires a high-photopic
317 level of illumination from the external light source (SI Appendix, Figs. S3 and S4).

318 The mechanism underlying the light-off-induced PKA activation is still unknown, but
319 we suggest that this mechanism likely involves two different light-dependent pathways: a
320 PKA suppression pathway with fast kinetics and a PKA activation pathway with slow
321 kinetics (Fig. 6G). Rhodopsin-containing wild-type PKAchu retinas showed transient
322 PKA suppression during the 10 min light-on period followed by immediate and robust
323 PKA activation upon light-off (Fig. 6F, SI Appendix, Movie S9). In contrast, the albino
324 PKAchu explants showed persistent PKA suppression during the 10 min light-on period
325 (Fig. 6F, SI Appendix, Movie S9). Because rhodopsin was not detected in the albino
326 retinal explant (Fig. 6A), this persistent suppression is likely to be mediated by the light-
327 induced dopamine release that can be triggered by cone visual pigments and/or
328 melanopsin in intrinsically photosensitive retinal ganglion cells (15) [but see (14)]. We
329 speculate that the persistent PKA suppression also operates in wild-type mice during the
330 light-on period, but that its presence is masked by rhodopsin-mediated PKA activation.

331 The fast kinetics of the suppression pathway is supported by the observation that the PKA
 332 activity is restored immediately after light-off in the albino PKAchu (Fig. 6F).

333 Rhodopsin and transducin play critical roles in the light-off-induced PKA activation
 334 (Fig. 4). Isorhodopsin is detected in the retina (Fig. 5E), but is not necessarily required for
 335 the light-off-induced PKA activation, because the response was also observed in dark-
 336 adapted PKAchu retinas devoid of 9-*cis* retinal (Figs. 2C and 5F). Conventional
 337 phototransduction, which utilizes the cGMP system (1-3), is also not likely to underlie the
 338 mechanism by the two reasons. First, the working light intensity of the light-off-induced
 339 PKA activation (SI Appendix, Fig. S3 A and B) is $>10^4$ -fold higher than that of the rod
 340 visual transduction (48). Second, the duration of the light-off-induced PKA activation is
 341 >10 min (Fig. 3); this is clearly longer than that of the visual photoresponse, which ends
 342 in a few seconds (48). Therefore, we speculate the presence of an alternative pathway
 343 acting downstream of transducin. Because the light-off-induced PKA activation is strictly
 344 confined within the illuminated region (Fig. 3 A-C, SI Appendix, Movie S6), intercellular
 345 signaling mechanisms may be excluded from this process.

346 One possible mechanism underlying the transducin-mediated PKA activation is the
 347 light-dependent transducin translocation. The Ca^{2+} -insensitive AC isoforms are enriched
 348 in the photoreceptor inner segment (53). It is suggested that transducin stimulates AC in
 349 primary culture of tiger salamander rods (43). Rod transducin is localized in the outer
 350 segment in darkness, but moves to the inner segment under bright light. This
 351 translocation contributes to the rod survival and synaptic transmission to rod bipolar cells
 352 (54), and is suggested to be a mechanism to escape from rod saturation (55). The
 353 transducin translocation occurs under the light level that saturates rod photoresponse with
 354 a half-time of completion of 5 and 12.5 min for α and β subunits, respectively (56) (57).
 355 These features coincide with the high half-saturation light intensity (SI Appendix, Fig.
 356 S3) and time course (Fig. 2) of the light-off-induced PKA activation. In addition, cone

357 transducin does not show the translocation (58), in line with the lack of the light-off-
358 induced PKA activation in cones (Fig. 3F). Interestingly, phosphorylation of phosducin,
359 one of the PKA targets in rods (21), facilitates the recovery from the translocation (59).
360 The transducin-mediated PKA activation may constitute a feedback loop to transducin for
361 the recovery from the translocation to boost the dark-adaptation.

362 The presence of isorhodopsin in our light-adapted retinal explants was unexpected
363 (Fig. 5). As a similar example, photoregeneration of isorhodopsin was reported
364 previously in frog retinal explants (60). In that case, the isorhodopsin was thought to be a
365 product of back photoconversion from a meta-intermediate of rhodopsin. It is tempting to
366 speculate that low-quantum yield isorhodopsin (61) plays a role in rod light-adaptation.
367 However, we suppose that isorhodopsin is not formed in the mouse retina *in vivo* because
368 9-*cis* retinal is not detected from retinoids directly extracted from light-adapted mouse
369 eyes (62). We speculate that isorhodopsin formation is an artifact caused by our sample
370 preparation, in which retinas were temporarily exposed to light at room temperature.

371 The maximum amplitude of the light-off-induced PKA activation became larger as
372 the light stimulus was shifted to longer wavelengths (SI Appendix, Fig. S3 B and C). As
373 the spectral sensitivity showed its maxima at 489 nm (Fig. 4A), this discrepancy suggests
374 the input from another photopigment(s) that independently regulates the amplitude.
375 Melanopsin displays a tristable photoequilibrium, and the fraction of its signaling form is
376 decreased as the wavelength becomes longer within the 400-600 nm range (63, 64).
377 Therefore, we speculate that red light-induced melanopsin inactivation increases the
378 amplitude of the light-off-induced PKA activation via the aforementioned dopamine-
379 mediated pathway.

380 Lastly, what is the physiological role of the light-off-induced PKA activation?
381 Previous biochemical studies have shown that PKA phosphorylates many
382 phototransduction components (19-22) and gap junction protein (24).

383 Electrophysiological studies have shown that cAMP improves the rod photosensitivity (11,
384 23). Taken together, these findings suggest that PKA promotes the dark-adaptation of
385 rods. In support of this notion, recent studies by Kolesnikov and colleagues reported a
386 delayed rod dark-adaptation in mutant mice whose GRK1 is mutated to block its cAMP-
387 dependent phosphorylation (65). PKA phosphorylates GRK1 to reduce its rhodopsin
388 phosphorylation ability (19), which in turn extends the active lifetime of rhodopsin to
389 increase the photosensitivity. They also reported lack of phenotype in cone dark-
390 adaptation, which is consistent with the lack of responses in our PKAchu cones (Fig. 3 *F*
391 and *G*). Therefore, we speculate that the physiological role of the light-off-induced PKA
392 activation is the acceleration of rod dark-adaptation upon the transition from a light to a
393 dark environment. Further physiological studies will be needed to quantitatively describe
394 the contribution of PKA in rod dark-adaptation.

395

396 **Materials and Methods**

397 **Animals.** Colonies of wild-type PKAchu (nbio185; NIBIOHN) and PKAchu-NC
398 (nbio186) transgenic mouse lines were maintained in heterozygous state on the B6J
399 background. Albino PKAchu was obtained by crossing with B6 albino (Charles River
400 Laboratories Japan). PKAchu *Gnat1*^{+/-} and PKAchu *Gnat1*^{-/-} were obtained by crossing
401 wild-type PKAchu with *Gnat1*^{-/-} (B6J background; the kind gift from Dr. Vladimir J
402 Kefalov) for 2-3 generations.

403 **Two-photon live imaging of the retinal explant.** A flat-mounted retina was perfused
404 with oxygenated medium and imaged with an upright multi-photon microscope system
405 (Fluoview FV1000MPE; Olympus) using a water immersion objective lens
406 (XLPLN25XWMP; Olympus). Stimulation light was generated with a custom-made LED
407 system (SI Appendix, Fig. S4) and delivered to the retina through the objective lens.

408 All additional experimental details are provided in *SI Appendix, Supplementary*
409 *Methods*.
410
411 **Acknowledgements**
412 Support was received in the form of the following: JSPS KAKENHI Grant (nos.
413 15H05949 “Resonance Bio” to M.M., 16H06280 “ABiS” to M.M., 19H00993 to M.M.;
414 and 19K16087 to S.S.); JST CREST “OptoBio” (nos. JPMJCR1654 to M.M. and
415 JPMJCR1753 to T.Y.); AMED (no. 19gm5010003h0003 to M.M.); The Shimizu
416 Foundation for Immunology and Neuroscience Grant for 2017 (S.S.); The Kyoto
417 University Research Fund for Young Scientists (Start-up) FY2017 (S.S.); The Kyoto
418 University Foundation (S.S.). The authors acknowledge the technical assistance of the
419 machine shop in Kyoto University. The authors thank Dr. Vladimir J Kefalov
420 (Washington University in St. Louis) for providing *Gnat1*^{-/-} mice and for his helpful
421 discussions and comments on the manuscript.
422

423 **References**

- 424 1. S. Kawamura, S. Tachibanaki, Rod and cone photoreceptors: molecular basis of the
425 difference in their physiology. *Comp Biochem Physiol A Mol Integr Physiol* **150**, 369-377
426 (2008).
- 427 2. G. L. Fain, R. Hardie, S. B. Laughlin, Phototransduction and the evolution of
428 photoreceptors. *Curr Biol* **20**, R114-124 (2010).
- 429 3. T. D. Lamb, Evolution of phototransduction, vertebrate photoreceptors and retina. *Prog*
430 *Retin Eye Res* **36**, 52-119 (2013).
- 431 4. K. W. Yau, R. C. Hardie, Phototransduction motifs and variations. *Cell* **139**, 246-264
432 (2009).
- 433 5. L. Astakhova, M. Firsov, V. Govardovskii, Activation and quenching of the
434 phototransduction cascade in retinal cones as inferred from electrophysiology and
435 mathematical modeling. *Mol Vis* **21**, 244-263 (2015).
- 436 6. X. H. Wen, A. M. Dizhoor, C. L. Makino, Membrane guanylyl cyclase complexes shape
437 the photoresponses of retinal rods and cones. *Front Mol Neurosci* **7**, 45 (2014).
- 438 7. O. P. Gross, E. N. Pugh Jr., M. E. Burns, cGMP in mouse rods: the spatiotemporal
439 dynamics underlying single photon responses. *Front Mol Neurosci* **8**, 6 (2015).
- 440 8. F. Vinberg, J. Chen, V. J. Kefalov, Regulation of calcium homeostasis in the outer
441 segments of rod and cone photoreceptors. *Prog Retin Eye Res* **67**, 87-101 (2018).
- 442 9. J. Zang, S. C. F. Neuhauss, The binding properties and physiological functions of
443 recoverin. *Front Mol Neurosci* **11**, 473 (2018).
- 444 10. Senin, II, K. W. Koch, M. Akhtar, P. P. Philippov, Ca²⁺-dependent control of rhodopsin
445 phosphorylation: recoverin and rhodopsin kinase. *Adv Exp Med Biol* **514**, 69-99 (2002).
- 446 11. L. A. Astakhova, D. A. Nikolaeva, T. V. Fedotkina, V. I. Govardovskii, M. L. Firsov,
447 Elevated cAMP improves signal-to-noise ratio in amphibian rod photoreceptors. *J Gen*
448 *Physiol* **149**, 689-701 (2017).
- 449 12. E. Popova, Role of dopamine in distal retina. *J Comp Physiol A Neuroethol Sens Neural*
450 *Behav Physiol* **200**, 333-358 (2014).
- 451 13. P. Witkovsky, Dopamine and retinal function. *Doc Ophthalmol* **108**, 17-40 (2004).
- 452 14. V. Pérez-Fernández *et al.*, Rod photoreceptor activation alone defines the release of
453 dopamine in the retina. *Curr Biol* **29**, 763-774 e765 (2019).
- 454 15. C. L. Prigge *et al.*, M1 ipRGCs influence visual function through retrograde signaling in
455 the retina. *J Neurosci* **36**, 7184-7197 (2016).

- 456 16. A. I. Cohen, R. D. Todd, S. Harmon, K. L. O'Malley, Photoreceptors of mouse retinas
457 possess D4 receptors coupled to adenylate cyclase. *Proc Natl Acad Sci U S A* **89**, 12093-
458 12097 (1992).
- 459 17. C. R. Jackson, S. S. Chaurasia, C. K. Hwang, P. M. Iuvone, Dopamine D(4) receptor
460 activation controls circadian timing of the adenylyl cyclase 1/cyclic AMP signaling
461 system in mouse retina. *Eur J Neurosci* **34**, 57-64 (2011).
- 462 18. K. A. Neve, J. K. Seamans, H. Trantham-Davidson, Dopamine receptor signaling. *J*
463 *Recept Signal Transduct Res* **24**, 165-205 (2004).
- 464 19. T. J. Horner, S. Osawa, M. D. Schaller, E. R. Weiss, Phosphorylation of GRK1 and
465 GRK7 by cAMP-dependent protein kinase attenuates their enzymatic activities. *J Biol*
466 *Chem* **280**, 28241-28250 (2005).
- 467 20. N. Balasubramanian, K. Levay, T. Keren-Raifman, E. Faurobert, V. Z. Slepak,
468 Phosphorylation of the regulator of G protein signaling RGS9-1 by protein kinase A is a
469 potential mechanism of light- and Ca²⁺-mediated regulation of G protein function in
470 photoreceptors. *Biochemistry* **40**, 12619-12627 (2001).
- 471 21. H. Song, M. Belcastro, E. J. Young, M. Sokolov, Compartment-specific phosphorylation
472 of phosducin in rods underlies adaptation to various levels of illumination. *J Biol Chem*
473 **282**, 23613-23621 (2007).
- 474 22. G. Wolbring, P. P. Schnetkamp, Modulation of the calcium sensitivity of bovine retinal
475 rod outer segment guanylyl cyclase by sodium ions and protein kinase A. *Biochemistry*
476 **35**, 11013-11018 (1996).
- 477 23. L. A. Astakhova, E. V. Samoiliuk, V. I. Govardovskii, M. L. Firsov, cAMP controls rod
478 photoreceptor sensitivity via multiple targets in the phototransduction cascade. *J Gen*
479 *Physiol* **140**, 421-433 (2012).
- 480 24. H. Li *et al.*, Adenosine and dopamine receptors coregulate photoreceptor coupling via
481 gap junction phosphorylation in mouse retina. *J Neurosci* **33**, 3135-3150 (2013).
- 482 25. P. H. Li, J. Verweij, J. H. Long, J. L. Schnapf, Gap-junctional coupling of mammalian
483 rod photoreceptors and its effect on visual detection. *J Neurosci* **32**, 3552-3562 (2012).
- 484 26. A. Goto *et al.*, Circuit-dependent striatal PKA and ERK signaling underlies rapid
485 behavioral shift in mating reaction of male mice. *Proc Natl Acad Sci U S A* **112**, 6718-
486 6723 (2015).
- 487 27. T. Yamaguchi *et al.*, Role of PKA signaling in D2 receptor-expressing neurons in the
488 core of the nucleus accumbens in aversive learning. *Proc Natl Acad Sci U S A* **112**,
489 11383-11388 (2015).

- 490 28. R. Mizuno *et al.*, In vivo imaging reveals PKA regulation of ERK activity during
491 neutrophil recruitment to inflamed intestines. *J Exp Med* **211**, 1123-1136 (2014).
- 492 29. Y. Kamioka *et al.*, Live imaging of protein kinase activities in transgenic mice expressing
493 FRET biosensors. *Cell Struct Funct* **37**, 65-73 (2012).
- 494 30. N. Komatsu *et al.*, Development of an optimized backbone of FRET biosensors for
495 kinases and GTPases. *Mol Biol Cell* **22**, 4647-4656 (2011).
- 496 31. M. A. Samuel, Y. Zhang, M. Meister, J. R. Sanes, Age-related alterations in neurons of
497 the mouse retina. *J Neurosci* **31**, 16033-16044 (2011).
- 498 32. C. Behrens, T. Schubert, S. Haverkamp, T. Euler, P. Berens, Connectivity map of bipolar
499 cells and photoreceptors in the mouse retina. *Elife* **5** (2016).
- 500 33. L. V. Johnson, G. S. Hageman, J. C. Blanks, Interphotoreceptor matrix domains ensheath
501 vertebrate cone photoreceptor cells. *Invest Ophthalmol Vis Sci* **27**, 129-135 (1986).
- 502 34. J. Zhang, Y. Ma, S. S. Taylor, R. Y. Tsien, Genetically encoded reporters of protein
503 kinase A activity reveal impact of substrate tethering. *Proc Natl Acad Sci U S A* **98**,
504 14997-15002 (2001).
- 505 35. K. Aoki, M. Matsuda, Visualization of small GTPase activity with fluorescence
506 resonance energy transfer-based biosensors. *Nat Protoc* **4**, 1623-1631 (2009).
- 507 36. D. Mustafi *et al.*, Transcriptome analysis reveals rod/cone photoreceptor specific
508 signatures across mammalian retinas. *Hum Mol Genet* **25**, 4376-4388 (2016).
- 509 37. D. G. McMahon, P. M. Iuvone, G. Tosini, Circadian organization of the mammalian
510 retina: From gene regulation to physiology and diseases. *Progress in Retinal and Eye*
511 *Research* **39**, 58-76 (2014).
- 512 38. P. Farshi, B. Fyk-Kolodziej, D. M. Krolewski, P. D. Walker, T. Ichinose, Dopamine D1
513 receptor expression is bipolar cell type-specific in the mouse retina. *J Comp Neurol* **524**,
514 2059-2079 (2016).
- 515 39. A. I. Cohen, C. Blazynski, Dopamine and its agonists reduce a light-sensitive pool of
516 cyclic AMP in mouse photoreceptors. *Vis Neurosci* **4**, 43-52 (1990).
- 517 40. I. Nir *et al.*, Dysfunctional light-evoked regulation of cAMP in photoreceptors and
518 abnormal retinal adaptation in mice lacking dopamine D4 receptors. *J Neurosci* **22**, 2063-
519 2073 (2002).
- 520 41. C. R. Jackson *et al.*, Essential roles of dopamine D4 receptors and the type 1 adenylyl
521 cyclase in photic control of cyclic AMP in photoreceptor cells. *J Neurochem* **109**, 148-
522 157 (2009).
- 523 42. Z. Cheng, Y. M. Zhong, X. L. Yang, Expression of the dopamine transporter in rat and
524 bullfrog retinas. *Neuroreport* **17**, 773-777 (2006).

- 525 43. P. D. Alfinito, E. Townes-Anderson, Activation of mislocalized opsin kills rod cells: a
526 novel mechanism for rod cell death in retinal disease. *Proc Natl Acad Sci U S A* **99**, 5655-
527 5660 (2002).
- 528 44. J. Wang, N. Zhang, A. Beuve, E. Townes-Anderson, Mislocalized opsin and cAMP
529 signaling: a mechanism for sprouting by rod cells in retinal degeneration. *Invest*
530 *Ophthalmol Vis Sci* **53**, 6355-6369 (2012).
- 531 45. V. I. Govardovskii, N. Fyhrquist, T. Reuter, D. G. Kuzmin, K. Donner, In search of the
532 visual pigment template. *Vis Neurosci* **17**, 509-528 (2000).
- 533 46. J. Fan, B. Rohrer, G. Moiseyev, J. X. Ma, R. K. Crouch, Isorhodopsin rather than
534 rhodopsin mediates rod function in RPE65 knock-out mice. *Proc Natl Acad Sci U S A*
535 **100**, 13662-13667 (2003).
- 536 47. P. D. Calvert *et al.*, Phototransduction in transgenic mice after targeted deletion of the rod
537 transducin alpha -subunit. *Proc Natl Acad Sci U S A* **97**, 13913-13918 (2000).
- 538 48. S. Nymark, R. Frederiksen, M. L. Woodruff, M. C. Cornwall, G. L. Fain, Bleaching of
539 mouse rods: microspectrophotometry and suction-electrode recording. *J Physiol* **590**,
540 2353-2364 (2012).
- 541 49. G. H. Daly, J. M. DiLeonardo, N. R. Balkema, G. W. Balkema, The relationship between
542 ambient lighting conditions, absolute dark-adapted thresholds, and rhodopsin in black and
543 hypopigmented mice. *Vis Neurosci* **21**, 925-934 (2004).
- 544 50. A. T. Slominski *et al.*, "Sensing the environment: regulation of local and global
545 homeostasis by the skin's neuroendocrine system" in *Advances in Anatomy, Embryology*
546 *and Cell Biology*, P. Sutovsky, Ed. (Springer, 2012), vol. 212, chap. 2, pp. 7-26.
- 547 51. G. W. DeVries, A. I. Cohen, I. A. Hall, J. A. Ferrendelli, Cyclic nucleotide levels in
548 normal and biologically fractionated mouse retina: effects of light and dark adaptation. *J*
549 *Neurochem* **31**, 1345-1351 (1978).
- 550 52. T. Euler, K. Franke, T. Baden, "Studying a light sensor with light: multiphoton imaging
551 in the retina" in *Multiphoton Microscopy*, E. Hartveit, Ed. (Humana Press, 2019), vol.
552 148, chap. 10, pp. 225-250.
- 553 53. R. M. Abdel-Majid, F. Tremblay, W. H. Baldrige, Localization of adenylyl cyclase
554 proteins in the rodent retina. *Brain Res Mol Brain Res* **101**, 62-70 (2002).
- 555 54. A. Majumder *et al.*, Transducin translocation contributes to rod survival and enhances
556 synaptic transmission from rods to rod bipolar cells. *Proc Natl Acad Sci U S A* **110**,
557 12468-12473 (2013).
- 558 55. A. Tikidji-Hamburyan *et al.*, Rods progressively escape saturation to drive visual
559 responses in daylight conditions. *Nat Commun* **8**, 1813 (2017).

- 560 56. E. S. Lobanova *et al.*, Transducin translocation in rods is triggered by saturation of the
561 GTPase-activating complex. *J Neurosci* **27**, 1151-1160 (2007).
- 562 57. M. Sokolov *et al.*, Massive light-driven translocation of transducin between the two
563 major compartments of rod cells: a novel mechanism of light adaptation. *Neuron* **34**, 95-
564 106 (2002).
- 565 58. E. S. Lobanova *et al.*, Mechanistic basis for the failure of cone transducin to translocate:
566 why cones are never blinded by light. *J Neurosci* **30**, 6815-6824 (2010).
- 567 59. M. Belcastro *et al.*, Phosphorylation of phosducin accelerates rod recovery from
568 transducin translocation. *Invest Ophthalmol Vis Sci* **53**, 3084-3091 (2012).
- 569 60. T. Reuter, Photoregeneration of rhodopsin and isorhodopsin from metarhodopsin III in
570 the frog retina. *Vision Res* **16**, 909-917 (1976).
- 571 61. R. Hubbard, A. Kropf, The action of light on rhodopsin. *Proc Natl Acad Sci U S A* **44**,
572 130-139 (1958).
- 573 62. K. A. Lee, M. Nawrot, G. G. Garwin, J. C. Saari, J. B. Hurley, Relationships among
574 visual cycle retinoids, rhodopsin phosphorylation, and phototransduction in mouse eyes
575 during light and dark adaptation. *Biochemistry* **49**, 2454-2463 (2010).
- 576 63. T. Matsuyama, T. Yamashita, Y. Imamoto, Y. Shichida, Photochemical properties of
577 mammalian melanopsin. *Biochemistry* **51**, 5454-5462 (2012).
- 578 64. A. J. Emanuel, M. T. Do, Melanopsin tristability for sustained and broadband
579 phototransduction. *Neuron* **85**, 1043-1055 (2015).
- 580 65. A. V. Kolesnikov, J. D. Chrispell, S. Osawa, V. J. Kefalov, E. R. Weiss, Phosphorylation
581 at Serine 21 in G protein-coupled receptor kinase 1 (GRK1) is required for normal
582 kinetics of dark adaptation in rod but not cone photoreceptors. *FASEB J* **34**, 2677-2690
583 (2020).
- 584

585 **Figure legends**

586 **Figure 1** Two-photon imaging of the PKAchu retina. (A) Imaging setup. The isolated
 587 PKAchu retina was flat-mounted on a culture insert, perfused with DMEM/F12 medium
 588 and imaged using an upright two-photon microscope with a water immersion objective
 589 lens. (B-G) Fluorescent images obtained from the PKAchu retina at the ganglion cell
 590 layer (GCL; B), inner plexiform layer (IPL; C), inner nuclear layer (INL; D), outer
 591 plexiform layer (OPL; E), outer nuclear layer (ONL; F) and photoreceptor segments layer
 592 (PRS; G). Images were obtained by averaging CFP Ch and FRET Ch images. (H)
 593 Longitudinal view of the PKAchu retina. The image was reconstructed from z-stack
 594 images (214 planes with 1 μm z-intervals). White arrowheads indicate cone nuclei. Black
 595 arrowheads indicate z-positions of the cross-sectional images in (B)-(G), and an arrow
 596 indicates the z position from which the excitation laser power was attenuated to avoid
 597 detector saturation. (I) Cone labeling with PNA-rhodamine (magenta) overlaid with
 598 AKAR3EV signals (green).

599

600 **Figure 2** Basal PKA activities and light-induced PKA activity changes in the dark- and
 601 light-adapted PKAchu retinas. (A) Longitudinal PKA activity images. Arrowheads
 602 indicate the positions of each layer analyzed in (B). (B) FRET/CFP values obtained from
 603 each layer of the retina. Mean \pm SD, $n = 7$ and 18 measurements for light- and dark-
 604 adapted retinas, respectively. The numbers on the bars are p-values from Tukey-Kramer's
 605 test following a two-way ANOVA. (C) Time-lapse PKA activity images from dark- and
 606 light-adapted retinas. Images are cross-sectional views obtained at the PRS layer. An
 607 arrow indicates the timing of a 6 sec light stimulation (500 nm , $1.0 \times 10^7 \text{ photons } \mu\text{m}^{-2}$
 608 sec^{-1}). (D) Time courses of the PKA activity at the PRS layer in dark- and light-adapted
 609 retinas. Mean \pm SD ($n = 3$ and 8 measurements, respectively). (E) The early phase of the
 610 light response in light-adapted retinas. Mean \pm SD ($n = 5$). (F) Time-lapse PKA activity

611 images at the PRS layer in the light-adapted retina. Bars indicate the timing of a 10 min-
612 light stimulation (500 nm , $3.2 \times 10^7\text{ photons } \mu\text{m}^{-2}\text{ sec}^{-1}$). (G) Time course of the PKA
613 activity at the PRS layer. A dashed bar indicates the timing of light stimulation. Light was
614 temporarily turned off four times for image acquisitions (every 2 min, $<10\text{ sec}$ each).
615 Mean \pm SD ($n = 4$). Data points in (D), (E) and (F) were obtained every 2 min, 12 sec and
616 2 min, respectively.

617

618 **Figure 3** Spatial distribution of the light-off-induced PKA activation. (A) Time-lapse
619 PKA activity images from light-adapted PKAchu and PKAchu-NC retinal explants.
620 Images are cross-sectional views at the PRS layer. Light stimulation (dashed circle,
621 wavelength 500 nm , $1.0 \times 10^8\text{ photons } \mu\text{m}^{-2}\text{ sec}^{-1}$, 6 sec) was given just before 0 min
622 (arrow). Scale bar: $400\text{ }\mu\text{m}$. (B) Positions of four areas analyzed in (C). (C) Time courses
623 of the $\Delta\text{FRET}/\text{CFP}$ in the 6 sec -stimulation experiments. Values are the means of five
624 (PKAchu) and three (PKAchu-NC) measurements. (D) Longitudinal view of the light-
625 induced PKA activation toward 6 sec stimulation (500 nm , $1.0 \times 10^8\text{ photons } \mu\text{m}^{-2}\text{ sec}^{-1}$).
626 Images were reconstructed from a z-stack of 61 images with $3\text{ }\mu\text{m}$ z-intervals. White
627 arrowheads show cones. Black arrowheads indicate the layer positions analyzed in (E).
628 (E) Time courses of the light-induced PKA activity change at the four indicated layers.
629 Values are the mean of four measurements. (F) High-magnification cross-sectional view
630 of the light-off-induced PKA activation at the PRS layer. Images were obtained before
631 and after the 6 sec stimulation (500 nm , $1.0 \times 10^8\text{ photons } \mu\text{m}^{-2}\text{ sec}^{-1}$). White arrowheads
632 indicate cones. (G) Time courses of the light-induced PKA activity change in rods (black)
633 and cones (cyan), in the 6 sec -stimulation experiments. Rod and cone signals were
634 separated by intensity-based image segmentation. Values are the mean \pm SD ($n = 8$
635 measurements). Data points in (C), (E), and (G) were obtained every 2 min. An arrow in
636 each panel indicates the timing of light stimulation.

637

638 **Figure 4** Involvement of rhodopsin and transducin in the light-off-induced PKA
 639 activation. (A) Spectral sensitivity plot of the light-induced rod PKA activation. Plots
 640 were fitted with the spectral template of the visual pigment to obtain the estimated λ_{\max} of
 641 489 nm (dashed curve). Data were normalized to the peak of the curve. Values are the
 642 mean \pm SEM (n = 3 to 7). (B) Time courses of the PKA activity in the 6 sec-stimulation
 643 experiments, obtained from rods imaged at PRS in wild-type PKAchu, PKAchu *Gnat1*^{+/-}
 644 and PKAchu *Gnat1*^{-/-}. Data for wild-type PKAchu is a replot of Fig. 3G. An arrow in
 645 each panel indicates the timing of light stimulation (500 nm, 1×10^8 photons μm^{-2} , 6 sec).
 646 Values are the mean \pm SD (n = 9 for PKAchu *Gnat1*^{+/-} and n = 18 for PKAchu *Gnat1*^{-/-}).
 647

648 **Figure 5** Formation of isorhodopsin in the light-adapted retinal explant. (A) Difference
 649 absorption spectra of retinal photopigments measured at 4 °C. Solid curve: light-adapted
 650 retinal explants, dashed curve: dark-adapted control. Values are the average of three
 651 measurements. Each sample was prepared from one retina. (B) Normalized spectra
 652 created from the data in (A). (C) A comparison between the difference absorption
 653 spectrum of the light-adapted retina (red) and the spectral sensitivity data (open circles,
 654 replot of Fig. 4A). Note that the vertical axis is in log scale. (D) Data fitting with
 655 rhodopsin (red) and isorhodopsin templates (cyan). The averaged spectrum of the light-
 656 adapted retina (solid black curve, replot from (A)) was fitted with the sum of the
 657 rhodopsin and isorhodopsin spectra (green). (E) HPLC chromatogram of retinoids
 658 extracted from a dark- or light-adapted retina. Retinal isomers were extracted as *syn*- and
 659 *anti*-oxime forms, separated by the normal phase HPLC, and detected by their absorbance
 660 at 360 nm. (F) Molar ratio of the retinoids estimated by HPLC. Values are the means of
 661 two and three measurements for dark- and light-adapted retinas, respectively. 11c: 11-*cis*
 662 retinal; at: all-*trans* retinal; 9c: 9-*cis* retinal; 13: 13-*cis* retinal; ROL: all-*trans* retinol.

663

664 **Figure 6** Basal PKA activity and light-induced PKA suppression in the albino PKAchu
 665 retina. (A) Difference absorption spectra of membrane proteins extracted from a wild-
 666 type (black) or an albino (red) mouse retina. Values are the means of three samples. (B)
 667 Longitudinal PKA activity images of wild-type and albino PKAchu retinas. Arrowheads
 668 indicate the positions of each layer analyzed in (C). (C) FRET/CFP values obtained from
 669 each layer of the retina. Mean \pm SD, $n = 7$ and 14 measurements for the wild-type and
 670 albino retinas, respectively. The number on the bar is a p-value from Tukey-Kramer's test
 671 following a two-way ANOVA. (D) Responses of rod PKA to 100 nM dopamine
 672 perfusion in wild-type (black) and albino (red) PKAchu retinas. Light-colored thin curves
 673 and dark-colored bold curves are individual and averaged data, respectively. (E, F).
 674 Light-induced PKA activity changes in response to 6 sec stimulation (E; 500 nm, $1.0 \times$
 675 10^8 photons $\mu\text{m}^{-2} \text{sec}^{-1}$) and 10 min stimulation (F; 500 nm, 3.2×10^7 photons $\mu\text{m}^{-2} \text{sec}^{-1}$).
 676 Albino data (red, mean \pm SD, $n = 4$ and 5 , respectively) are adjusted 0.16 upward from
 677 the wild-type data (dashed black) with consideration for the average difference in the
 678 basal FRET/CFP (PRS in (C)). Wild-type data are replots of Fig. 3G and Fig. 2G,
 679 respectively. Data points were obtained every 2 min. (G) A hypothetical model of the
 680 light-off-induced PKA activation. Green bars show the timing of a light stimulation.
 681

Figure 1

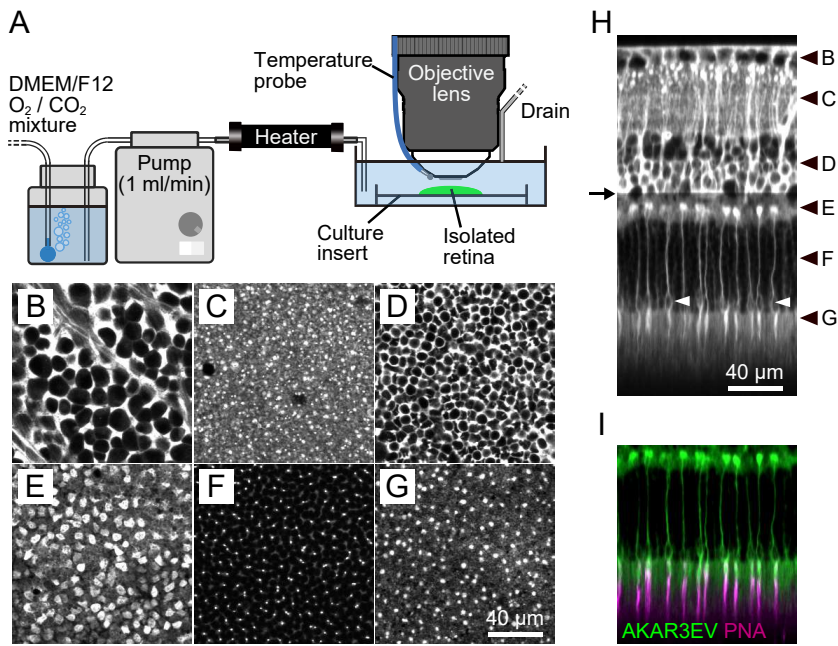


Figure 2

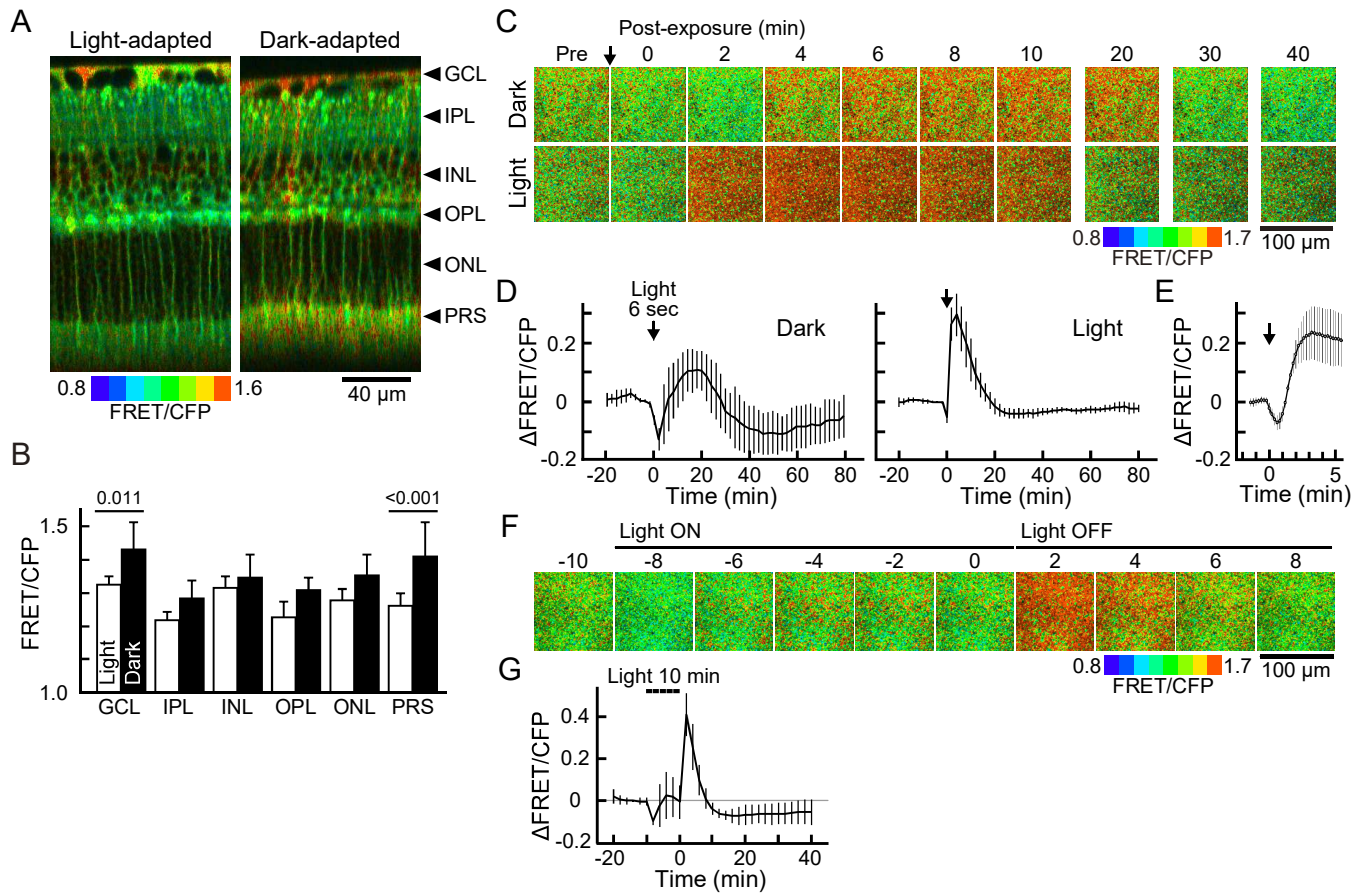


Figure 3

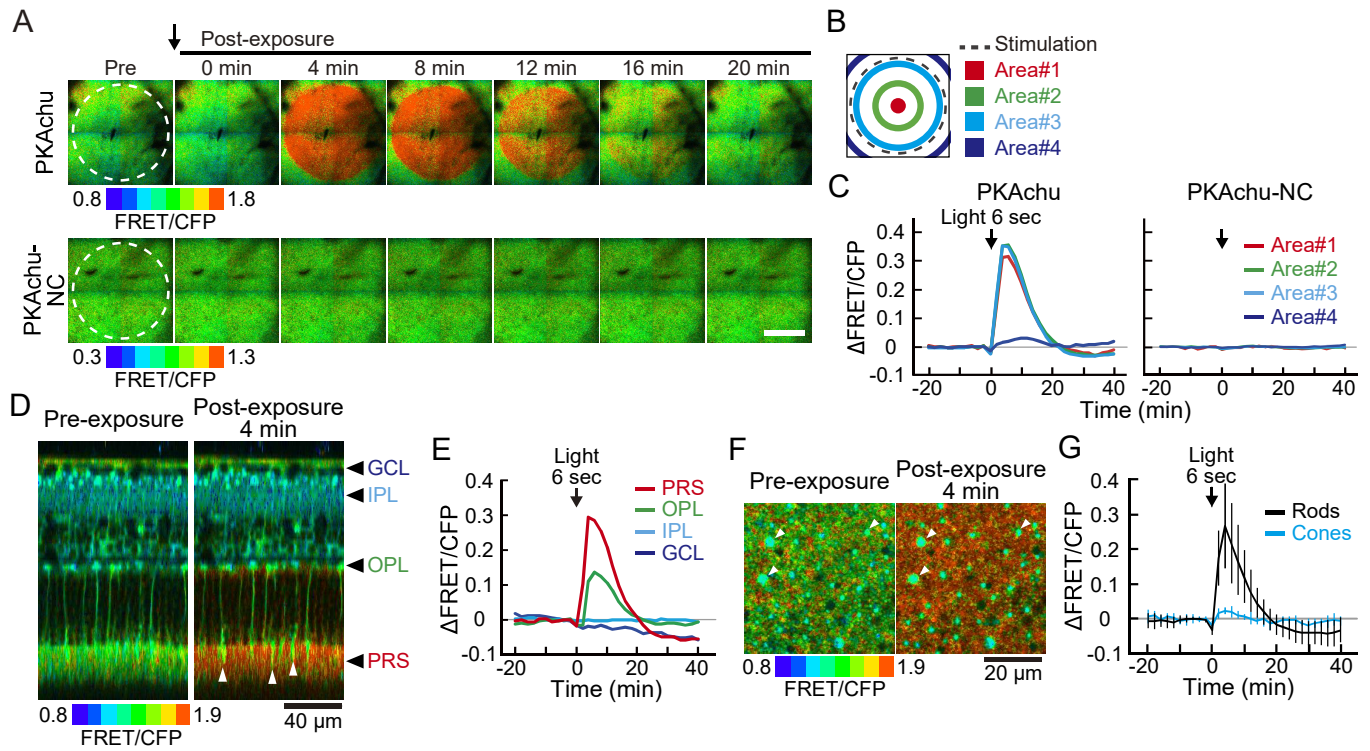


Figure 4

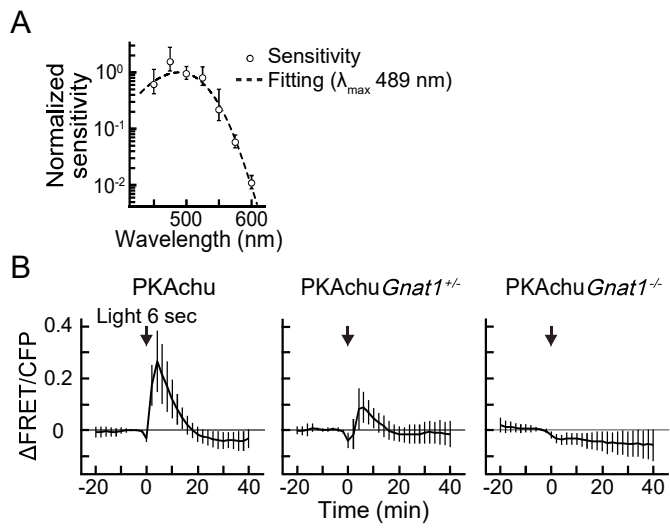


Figure 5

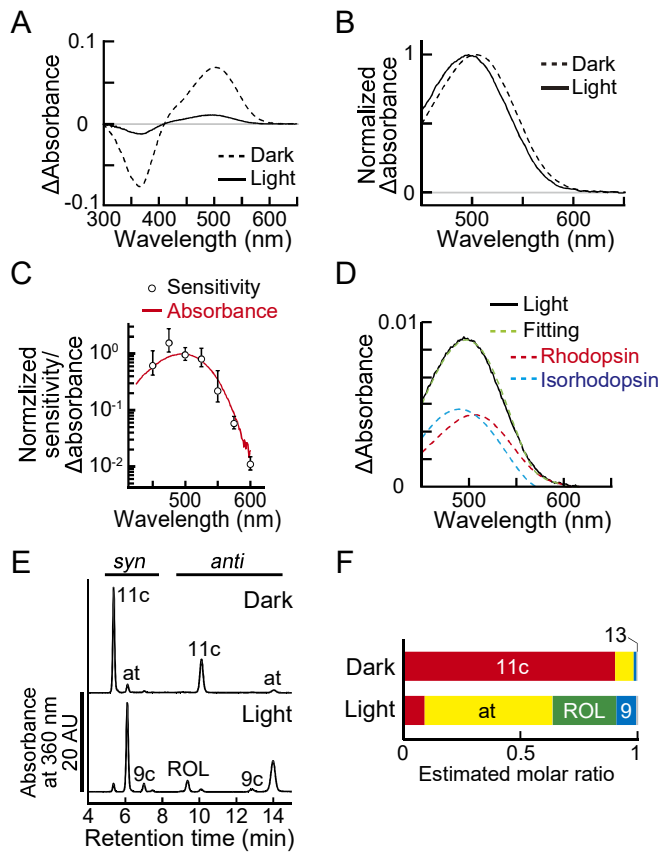
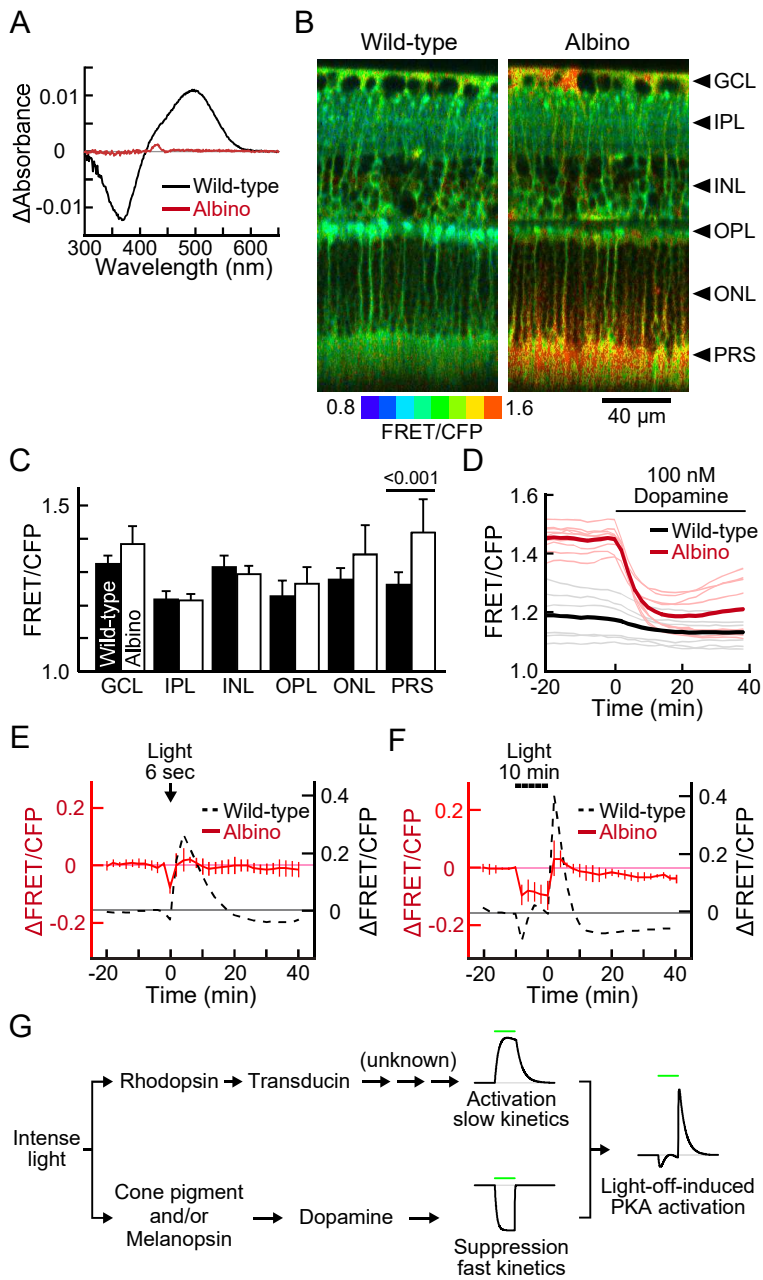


Figure 6



PNAS

www.pnas.org

1

2 Supplementary Information for

3 **Rhodopsin-mediated Light-off-induced Protein Kinase A Activation in**
4 **Mouse Rod Photoreceptor Cells.**

5 Shinya Sato^{a*}, Takahiro Yamashita^b, and Michiyuki Matsuda^{a,c}

6 ^aLaboratory of Bioimaging and Cell Signaling, Graduate School of Biostudies, Kyoto University, Kyoto
7 606-8501 Japan;

8 ^bDepartment of Biophysics, Graduate School of Science, Kyoto University, Kyoto 606-8502 Japan;

9 ^cDepartment of Pathology and Biology of Diseases, Graduate School of Medicine, Kyoto University, Kyoto
10 606-8501 Japan;

11 *To whom correspondence should be addressed: Shinya Sato

12 **Address:** Laboratory of Bioimaging and Cell Signaling, Graduate School of Biostudies, Kyoto University,
13 Kyoto 606-8501 Japan;

14 **TEL:** +81-75-753-9450

15 **Email:** sato.shinya.7e@kyoto-u.ac.jp

16

17 **This PDF file includes:**

18 Supplementary Text

19 Supplementary Methods

20 Figures S1 to S4

21 Legends for Movies S1 to S9

22 SI References

23

24 **Other supplementary materials for this manuscript include the following:**

25 Movies S1 to S9

26

27 **Supplementary Text**

28 **Estimated amount of photopigment activation by two-photon imaging.**

29 There are three pathways for the rhodopsin activation and bleaching during two-photon
30 imaging; direct single-photon and two-photon activations by the excitation light (direct
31 1P excitation, direct 2P excitation), and an indirect excitation by the emission from the
32 fluorescent probe(s) (1). We have estimated the direct and indirect photopigment
33 activation rates in a single imaging scan as $4 \times 10^2 \text{ R}^* \text{ rod}^{-1}$ and $1 \times 10^3 \text{ R}^* \text{ rod}^{-1}$,
34 respectively. These values are clearly smaller than the values that are required for the
35 light-off-induced PKA activation.

36 We will describe how these rates were obtained. First, we estimated the direct 1P and
37 2P activations in our typical imaging set up using the light-adapted retinal explant. Based
38 on the spectral sensitivity of the mouse rod in the infrared region (2), we assumed that the
39 1P excitation is dominant at 800 nm, whereas the 2P excitation becomes dominant at 900
40 nm. Unfortunately, sensitivity at 840 nm, which was used in our study, was not reported.
41 Although the ratio of contribution is not clear, here, we assumed that 1P and 2P
42 excitations have comparable contributions at 840 nm.

43 The Govardovskii template (3) was used to estimate the 1P activation efficiency.
44 When the rhodopsin template (λ_{max} 500 nm) is extended to 840 nm, the relative
45 absorbance efficiency is 2.4×10^{-9} to the maximum (Fig. S5A). The excitation laser
46 power in our typical imaging was 8 mW at the sample plane. The power of photon at 840
47 nm is 2.4×10^{-19} (J), which is obtained from the equation $E = hc/\lambda$, where E is the energy
48 of a photon, h is the plank constant ($6.62607015 \times 10^{-34}$), c is the speed of light in
49 vacuum ($3.0 \times 10^8 \text{ m sec}^{-1}$), and λ is the wavelength ($8.4 \times 10^{-7} \text{ m}$). Thus, the average
50 photon flux of the excitation laser is $(8.0 \times 10^{-3}) / (2.4 \times 10^{-19}) \approx 3.3 \times 10^{16} \text{ photons sec}^{-1}$,
51 and the photon density at the sample, based on the pixel dwelling time (8 μsec) and the
52 pixel size ($0.17 \mu\text{m}^2$), is $(3.3 \times 10^{16}) \times (8 \times 10^{-6}) / (0.17) \approx 1.6 \times 10^{12} \text{ photons } \mu\text{m}^{-2}$. Using
53 the relative absorbance efficiency above, the 1P excitation in one scan of 840 nm laser is

54 comparable to $(1.6 \times 10^{12}) \times (2.4 \times 10^{-9}) \approx 3.8 \times 10^3$ photons μm^{-2} flash of 500 nm light.
 55 By multiplying the collecting area of a mouse rod, $0.47 \mu\text{m}^2$ (4), rhodopsin activation was
 56 estimated as $1.8 \times 10^3 \text{ R}^* \text{ rod}^{-1}$, when the retina is dark-adapted and contains ~100%
 57 rhodopsin. However, in our light-adapted retinal explant, unbleached photopigments were
 58 approximately 8% rhodopsin and 8% isorhodopsin (Fig. 5D). Quantum yield of
 59 isorhodopsin is about 1/3 of rhodopsin (5). Therefore, estimated 1P excitation in our
 60 light-adapted retinal explant is $(1.8 \times 10^3) \times (0.08 + 0.08/3) \approx 1.9 \times 10^2 \text{ R}^* \text{ rod}^{-1}$.
 61 Assuming that 1P and 2P excitations have comparable contributions, we estimated the
 62 total direct excitation rate as approximately $4 \times 10^2 \text{ R}^* \text{ rod}^{-1}$.

63 Next, we estimated the indirect activation. Because imaging was mainly done from
 64 PRS, we assumed that the AKAR3EV fluorescence is absorbed by rhodopsin without any
 65 attenuation. To obtain the relationship between photon emission and the pixel intensity of
 66 fluorescent image, calibrated 475 nm or 535 nm light from the light stimulation device
 67 (Fig. S4) was injected directly into the objective lens (Fig. S5B), and the light was
 68 detected with the CFP Ch detector (460-500 nm) or FRET Ch detector (520-560 nm),
 69 respectively, with an 8 μsec of the pixel dwelling time (Fig. S5C). Then, mean intensities
 70 of images were plotted as a function of the photon number per pixel (Fig. S5D). Using
 71 this relationship, a mean CFP Ch pixel intensity in our typical imaging, 300, was
 72 converted to 6×10^2 photons pixel^{-1} . The FRET Ch sensitivity was 94% of the CFP Ch
 73 sensitivity; this value will be used later for a calibration.

74 In the real specimen, fluorescent emission is supposed to be radiated toward random
 75 directions so that only a part of them are collected by the objective lens. Based on the
 76 numerical aperture of the objective lens (1.05) and the refractive index of the DMEM/F12
 77 medium (1.34), the objective aperture angle is calculated as 0.90 radians, and the fraction
 78 of the photon collection was estimated as $(0.90 \times 2) / (2\pi) \approx 0.29$. Thus, the estimated
 79 total photon emission from the AKAR3EV is $(6 \times 10^2) / 0.29 \approx 2 \times 10^3$ photons pixel^{-1} .

80 Because the photon number so far is estimated only for those detected by the CFP Ch
 81 detector (i.e. photons in 460-500 nm range), we expanded this for the whole emission
 82 spectrum of the AKAR3EV. The emission spectrum of the AKAR3EV was predicted by
 83 summing up those of mTurquoise and YPet (Fig. S5E) which comprise AKAR3EV. The
 84 YPet spectrum was then scaled based on the basal FRET/CFP of PRS layer (1.24; Fig.
 85 2B, PRS of the light-adapted retina). Considering the detector sensitivity ratio above, the
 86 ratio of the area corresponding to FRET Ch and CFP Ch was adjusted at $1.24 / 0.94 =$
 87 1.32. The whole spectrum was further scaled up to set the area for the CFP Ch to the
 88 above estimated photon number, 2×10^3 (Fig. S5F). Finally, the effect of the AKAR3EV
 89 fluorescence on the rhodopsin activation was estimated by multiplying the normalized
 90 absorbance spectrum of rhodopsin (Fig. S5G), which converts the photon number of each
 91 wavelength into the corresponding number at 500 nm. The area of this calibrated
 92 spectrum is comparable to 5×10^3 photons pixel⁻¹ of 500 nm light (Fig. S5H). Using the
 93 pixel size ($0.17 \mu\text{m}^2$), this value was converted to $(5 \times 10^3) / (0.17) \approx 3 \times 10^4$ photons μm^{-2} .
 94 Using the collecting area ($0.47 \mu\text{m}^2$) and the fractions of rhodopsin and isorhodopsin in
 95 our light-adapted retinal explant (8% each), the value was further converted as described
 96 earlier, to obtain the total indirect excitation rate of 1×10^3 R* rod⁻¹.

97 The photon density estimated for direct and indirect activations are in the order of 10^3
 98 and 10^4 photons μm^{-2} , respectively, at 500 nm. On the other hand, the half saturating light
 99 intensity of the light-off-induced PKA activation was 6.5×10^7 photons μm^{-2} at 500 nm
 100 (Fig. S3B). Therefore, the impact of imaging technique is thought to be negligible, at
 101 least on the PKA activation.

102

103 **Supplementary Methods**

104 **Ethical approval.** The animal protocols were reviewed and approved by the Animal Care
105 and Use Committee of Kyoto University Graduate School of Medicine (MedKyo17539,
106 17539-2, 18086, 19090, and 20081) and methods were carried out in accordance with the
107 relevant guidelines and regulations.

108

109 **Reagents.** Dulbecco's modified Eagle's medium/nutrient mixture F-12 Ham
110 (DMEM/F12; D2906, Sigma-Aldrich, St. Louis, MO, USA) supplemented with 1% (v/v)
111 Penicillin-Streptomycin (26253-84; Nacalai Tesque, Kyoto, Japan) was prepared just
112 before the imaging experiment. The medium was warmed up in a 40 °C water bath and
113 bubbled with an O₂ and CO₂ gas mixture. The pH was monitored with a pH tester
114 (HI98100; HANNA Instruments, Woonsocket, RI, USA), and the CO₂ concentration was
115 adjusted to obtain pH 7.2-7.4. For the cone-specific staining in Fig. 1I, PNA-rhodamine
116 (RL-1072; Vector Laboratories, Burlingame, CA, USA) was added to DMEM/F12
117 medium at 0.2% (v/v). Forskolin (F-500; Alomone Labs, Jerusalem, Israel) was dissolved
118 in dimethyl sulfoxide (DMSO) at 50 mM and kept at -20 °C until used. Dopamine (040-
119 15433; FUJIFILM Wako Pure Chemical, Osaka, Japan) was dissolved in ultrapure water
120 at 1 mM and kept at -80 °C until used. 4-(2-hydroxyethyl)-1-piperazineethanesulfonic
121 acid (HEPES) and NaCl were purchased from Nacalai Tesque. NaOH and hydroxylamine
122 hydrochloride were from FUJIFILM Wako Pure Chemical. *n*-Dodecyl-β-D-maltoside
123 (DDM) was from Dojindo (Kumamoto, Japan). Reagents for retinoid extraction and
124 HPLC analysis (dichloromethane, *n*-hexane, Na₂SO₃, diethyl ether, isopropanol and
125 benzene) were from FUJIFILM Wako and Nacalai Tesque. The genomic DNA extraction
126 kit (69504; DNeasy Blood and Tissue Kit) was from Qiagen (Hilden, Germany). PCR
127 reagents were from TaKaRa Bio (Kusatsu, Japan) and Toyobo (Osaka, Japan). PCR
128 primers were from Fasmac (Atsugi, Japan).

129

130 **Animals.** Mice (*Mus musculus*) were housed in a specific-pathogen-free facility with a
131 14/10 hour light-dark cycle, fed a standard laboratory chow diet and water *ad libitum*, and
132 used at the age of 1–6 months. Both male and female mice were used. Two or more
133 animals were used for every experiment to confirm the reproducibility. PKAchu
134 (C57BL/6J (B6J) background, nbio185; NIBIOHN, Osaka, Japan) and PKAchu-NC
135 (C57BL/6J (B6J) background, nbio186) transgenic mice were backcrossed with B6
136 albino mice (Charles River Laboratories Japan, Yokohama, Japan) for more than 9
137 generations and used as albino PKAchu and albino PKAchu-NC, respectively.
138 Transgene-positive, heterozygous mice were selected by visual inspection of their body
139 fluorescence and used for both breeding and imaging. Wild-type PKAchu and PKAchu-
140 NC were generated by crossing those albino mice with normal pigmented B6J mice
141 (Charles River Laboratories Japan) for 3-7 generations, except for PKAchu used in the
142 experiment shown in Fig. 1, which was crossed for only 1 generation. Removal of both
143 the *rd8* mutation (a single base deletion at nt3481 on *Crb1*) (6) and the albino mutation (a
144 G291T point mutation on *Tyr*) (7) was verified by Sanger sequencing of genomic DNA
145 extracted using the DNeasy Blood and Tissue Kit (Qiagen). The following primers were
146 used: for *rd8* genotyping, 5'-ACCTGATGGGTTCCCAATTG-3' (forward) and 5'-
147 AACCAGCCTTGTTTAGCACC-3' (reverse); for albino genotyping, 5'-
148 GGGGTTGCTGGAAAAGAAGTCTGTG-3' (forward) and 5'-
149 TGTGGGGATGACATAGACTGAGCTG-3' (reverse). PKAchu *Gnat1*^{+/-} and PKAchu
150 *Gnat1*^{-/-} were obtained by crossing wild-type PKAchu with *Gnat1*^{-/-} mice (B6J
151 background; the kind gift of Dr. Vladimir J. Kefalov) (8) for 2-3 generations. For
152 genotyping *Gnat1*, genomic DNA was extracted by incubating a biopsy sample in 50 μ L
153 of 0.1 M NaOH (1 hour, 95 °C). The sample was then neutralized by adding 50 μ L of 1
154 M Tris-HCl (pH 7.5) and centrifuged (15300 \times g, 1 min, 25 °C). The resulting supernatant
155 was used as a template for a genotyping PCR. The following primers were used: for the
156 *Gnat1* wild-type allele, 5'-GGCTTTCTTCAGGGGTCTTA-3' (forward) and 5'-

157 GGCAGGGTAGTGGTTGTGAA-3' (reverse); for the *Gnat1* knockout allele, 5'-
158 CATTGACCAAGCGAAACATC-3' (forward) and 5'-
159 ATATCACGGGTAGCCAACGCTATG-3' (reverse). Taken together, the genetic
160 background of PKAchu and PKAchu-NC used in this study is normal pigmented B6J
161 except for albino PKAchu and PKAchu-NC that have the B6 albino background.

162

163 **Preparation of the retinal explants for imaging.** The following tools were used in the
164 retina dissection: a stereomicroscope (SZX16; Olympus, Tokyo), curved forceps (91197-
165 00; Fine Science Tools, Foster City, Canada), micro-scissors (15009-08; Fine Science
166 Tools) and two fine forceps (11251-20; Fine Science Tools). For dark-adapted retinas, a
167 mouse was kept in darkness overnight and the preparation was done under dim red light.
168 For light-adapted retinas, a mouse was kept under normal room illumination (white light,
169 200-300 lux) for more than 1 hour and the explants were prepared under the same
170 lighting condition. The relative amount of unbleached photopigments in this explant was
171 constantly about 16% to that of rhodopsin in the dark-adapted control for wild-type (Fig.
172 5A) and was below the detection limit for albino (Fig. 6A). If not otherwise specified,
173 imaging data were obtained from light-adapted retinal explants. A mouse was killed
174 under isoflurane anesthesia. Eyes were enucleated with curved forceps and hemisected to
175 remove the cornea, vitreous and lens. Eyecups thus obtained were transferred into a 35-
176 mm culture dish filled with 2 mL DMEM/F12 medium and cut radially from three or four
177 points. The retina was peeled off with fine forceps and transferred onto a culture insert
178 (PICMORG50; Merck Millipore, Billerica, MA, USA) which was pre-wet with
179 DMEM/F12. The retina was flat-mounted ganglion cell-side up and tightly adhered onto
180 the culture insert with suction (9) to prevent positional drift and detachment during time-
181 lapse imaging. The culture insert was then fixed in a custom perfusion chamber made of
182 acrylic glass (width 40 mm, depth 33 mm, height 10 mm) or a square polystyrene dish (1-
183 4698-01; As One, Osaka, Japan). The entire preparation process was completed in less

184 than 20 min after administration of anesthesia. For the cone-labeling in Fig. 1I, the
185 culture insert with a retinal explant was placed onto 1 mL DMEM/F12 supplemented
186 with 0.2% (v/v) PNA-rhodamine, pre-incubated in a humidified CO₂ incubator at 37 °C
187 for 1 hour and then washed once with DMEM/F12 just before the imaging (10).

188

189 **Perfusion equipment.** The perfusion chamber was placed on an electromotive
190 microscope stage (MPT-AS01-FV; SIGMA KOKI, Hidaka, Japan) with a heating pad
191 (MP-908-N; Makami Denshi, Kishiwada, Japan). The retina in the chamber was perfused
192 with oxygenated DMEM/F12 medium delivered at 1 mL/min using a double-head
193 peristaltic pump (AC-2110 II; ATTO, Tokyo) and warmed up with an inline heater (an
194 SF28 heater controlled by a TC344B temperature controller; Warner instruments,
195 Hamden, CT, USA) (Fig. 1A). Medium was continuously drained from the chamber with
196 the same pump. The drain rate was adjusted to be slightly higher than 1 mL/min to
197 prevent overflow. The heater voltage was adjusted manually to maintain the temperature
198 in the dish at 33-35 °C (11), which was monitored by a K-type thermocouple probe (AD-
199 1214; A&D, Tokyo) attached near the tip of the objective lens. Temperature data was
200 imported to a computer via a breakout board (MAX31855; Adafruit, New York, NY) and
201 an Arduino UNO microcontroller board (Arduino, Turin, Italy). Temperature was
202 recorded using a program modified from the MAX31855 library (Adafruit;
203 <https://github.com/adafruit/Adafruit-MAX31855-library>) or the Tera Term software
204 (<https://ttssh2.osdn.jp/index.html.en>).

205

206 **Two-photon microscopy.** The retina in the chamber was perfused with oxygenated
207 DMEM/F12 medium using the above-mentioned perfusion system. Imaging was done
208 with an upright multi-photon microscope system (Fluoview FV1000MPE; Olympus,
209 Tokyo) with a water immersion objective lens (XLPLN25XWMP; Olympus). A
210 Ti:Sapphire femtosecond laser (Mai-tai DeepSee HP; Spectra-Physics, Santa Clara, CA,

211 USA) was tuned at 840 nm and used for excitation. Laser power at the specimen was
212 adjusted within 5-10 mW. The specimen was XY-scanned at 256×256 pixels with 8
213 μ sec of pixel dwelling time. Fluorescent emission was collected by the objective lens,
214 filtered through a dichroic mirror RDM690 (Olympus) to block the returned excitation
215 light, split with a set of dichroic mirrors (DM505, DM450 and DM570; Olympus) and
216 finally filtered through bandpass filters (FF01-425/30-25; Semrock, Rochester, NY,
217 USA; BA460-500, Olympus; BA520-560, Olympus; 645/60, Chroma, Bellows Falls, VT,
218 USA) to separate blue (not used in this study), cyan (CFP Ch), yellow (FRET Ch) and red
219 fluorescence (Red Ch; used only for the rhodamine-labeled image in Fig. 1I),
220 respectively. Fluorescent signals were detected and amplified with multi-alkaline
221 photomultiplier tubes to reconstruct images on FV10-ASW software version 4.2
222 (Olympus). Images in Fig. 3A and Movie S5 were created by combining four $509 \mu\text{m}$
223 square images which were obtained sequentially within 30 sec.

224

225 **Light stimulation.** Stimulation light was generated with a custom-made LED system
226 (Fig. S4). Light intensity and duration were controlled by the Arduino UNO
227 microcontroller board connected to the LED driver, using a program written with
228 Arduino IDE. When necessary, calibrated neutral density filters (ND filters, Fig. S4;
229 Edmund Optics, Barrington, NJ, USA) were additionally used to attenuate the light
230 intensity. Light wavelength was controlled by a bandpass filter (Fig. S4; Edmund Optics).
231 Light was delivered to the retina through the objective lens. To avoid light attenuation,
232 the dichroic mirror RDM690 before the objective lens was manually changed to a normal
233 mirror during the stimulation. Light intensity was calibrated based on power
234 measurements with an optical power meter (TQ8210; Advantest, Tokyo). The power in
235 Watts was divided by the energy of a photon and illuminated area (0.68 mm^2 circle) to
236 obtain photon density. The energy of a photon was derived from

237

$$E = \frac{h\nu}{\lambda}$$

238

239

240

241

242

243

244

245

246

247

248

249

250

251

252

253

254

255

256

257

258

259

260

261

262

where E is photon energy, h is the Planck constant ($6.62606957 \times 10^{-34}$ m² kg sec⁻¹), c is the speed of light in a vacuum (2.99792458×10^8 m/sec) and λ is wavelength (m). For short stimulations, light was delivered in 6 sec just before an image acquisition, except for 6×10^{10} and 1.9×10^{11} (photons μm^{-2} sec⁻¹) stimulation at both 575 and 600 nm, in which the maximal light intensity was used for 6-30 sec to deliver the indicated numbers of photons. For long stimulations of 10 min (Figs. 2E and 6F), light was delivered only during the intervals of time-lapse imaging, and thus the light was temporarily turned off every 2 min during the image acquisition (< 10 sec). View fields for the light response measurements were always selected from areas where the stimulation light spot had not been projected yet.

Image analyses. Images were analyzed on Fiji (<https://fiji.sc>). Positional drift in the time-lapse imaging was corrected with the Correct 3D drift plug-in (12). The minimum pixel intensity obtained from a blank image was used as the background signal and subtracted from every pixel. Pseudocolor PKA activity images were generated by multiplying an 8-color FRET/CFP ratio image and the corresponding intensity-normalized grayscale image (Fig. S1B). Longitudinal images of the retina were created by reconstruction from z-stack images. Sixteen y-slice images were averaged for noise reduction and better visualization of cellular morphology. When comparing rods and cones (Fig. 3 F and G), intensity-based segmentation was performed using a mask image that covered the cone or rod region. The mask image was created by superimposing two binary images. The first image was created using the Auto threshold function with the MaxEntropy method (13). To create the second image, a local background image was created by applying a median filter of 10 pixels diameter, and this background image was subtracted from the original image. The subtracted image was then binarized into the top 1% highest intensity pixels

263 and others, to obtain the second binary image. Two mask images were overlaid using the
264 Image calculator function with the OR method. The thus-obtained mask image or its
265 inverted image was applied to the original image to extract cone or rod signals,
266 respectively.

267

268 **Photopigment analyses.** The absorbance spectrum of photopigments in the retina was
269 obtained as described previously (4). A dark-adapted control retina was transferred into
270 500 μL collection buffer (140 mM NaCl, 50 mM HEPES, pH 6.5 NaOH) immediately
271 after its collection and frozen with liquid nitrogen. A light-adapted retina was flat-
272 mounted as described above, transferred into 500 μL collection buffer and frozen. A
273 frozen retina was thawed and homogenized using a 1 mL syringe (SS-01T; Terumo,
274 Tokyo) by passing through a 23-gauge needle (NN-2325R; Terumo) and centrifuged
275 (17,400 $\times g$, 15 min, 4°C). After removing the supernatant, the membrane precipitate was
276 solubilized in 300 μL solubilization buffer (collection buffer supplemented with 1%
277 (w/v) DDM), mixed on a rotator at 4°C for 30 min, and centrifuged (17,400 $\times g$, 15 min,
278 4°C). The supernatant was collected, supplemented with 16 μL of 5 M NH_2OH (pH 6.8,
279 NaOH; final concentration of 100 mM) and analyzed with a spectrophotometer (UV-
280 2400PC; Shimadzu, Kyoto) at 4°C. The difference spectrum of photopigment was
281 obtained from absorbance data before and after an irradiation with intense yellow light
282 passed through a Y52 filter. Molar extinction coefficients of rhodopsin (40,200 $\text{M}^{-1} \text{cm}^{-1}$)
283 (14) and isorhodopsin (43,000 $\text{M}^{-1} \text{cm}^{-1}$) (15) were used to estimate the molar amount of
284 each pigment after the fitting analysis in Fig. 5D.

285 Equivalent DDM-solubilized samples were also used for the HPLC analysis. Retinoid
286 extraction and HPLC were performed as described previously (16) using an HPLC
287 system (LC-10AT VP; Shimadzu) with a silica column (150 \times 6.0 mm, A-012-3; YMC,
288 Kyoto, Japan) and a solvent composed of 98.8% (v/v) benzene, 1.0% (v/v) diethylether,
289 and 0.2% (v/v) 2-propanol. Each retinoid in eluate was detected by its absorbance at 360

290 nm. Molar ratios of retinoids were estimated by dividing the peak area with the
 291 corresponding molar extinction coefficient at 360 nm ($M^{-1} \text{ cm}^{-1}$): 35,000 for *syn*-11-*cis*
 292 retinal oxime; 29,600 for *anti*-11-*cis* retinal oxime; 54,900 for *syn*-all-*trans* retinal oxime;
 293 51,600 for *anti*-all-*trans* retinal oxime; 39,300 for *syn*-9-*cis* retinal oxime; 30,600 for
 294 *anti*-9-*cis* retinal oxime; 49,000 for *syn*-13-*cis* retinal oxime; 52,100 for *anti*-13-*cis*
 295 retinal oxime; and 10,900 for all-*trans* retinol.

296

297 **Data fittings.** Rhodopsin absorption (Fig. 5D) was fitted with rhodopsin and
 298 isorhodopsin templates from 450 to 600 nm by the least squares method. The rhodopsin
 299 template was experimentally obtained from the dark-adapted control retina, and the
 300 isorhodopsin template was obtained from the literature (17).

301 Intensity-response relationships (Fig. S3B) were fitted using Origin 9 (OriginLab,
 302 Northampton, MA, USA) with the Naka-Rushton equation:

$$303 \quad R = R_{max} \frac{I^n}{(I^n + I_{1/2}^n)}$$

304 where R is the peak amplitude, R_{max} is the amplitude of the saturated response, I is light
 305 intensity, n is the Hill coefficient, and $I_{1/2}$ is the light intensity to generate a half-maximal
 306 response.

307 A spectral sensitivity plot (Fig. 4A) was fitted with the spectral template for the α -
 308 band of A1 pigments:

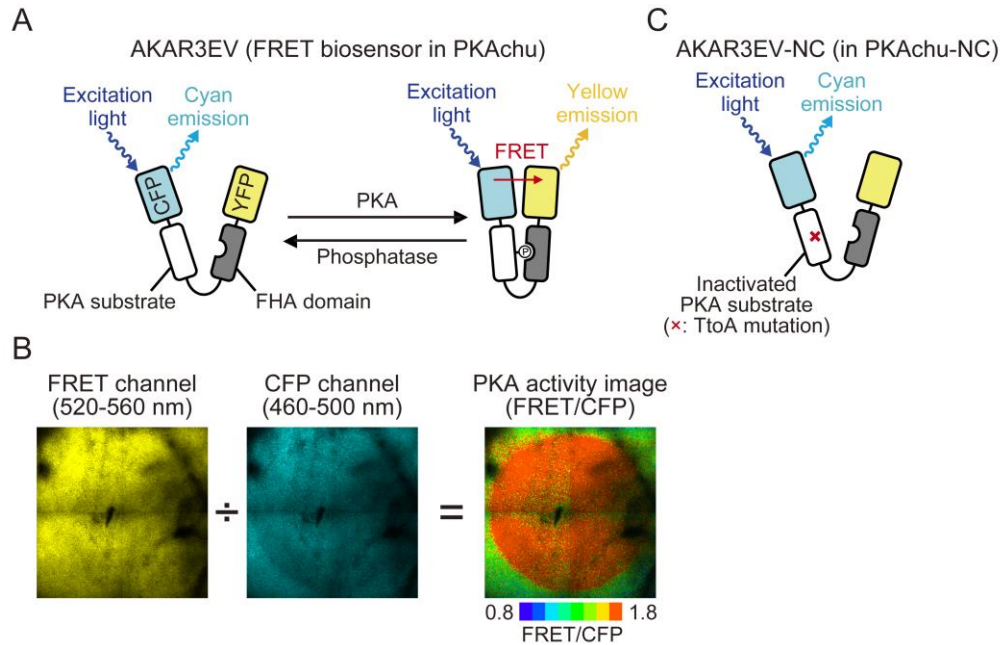
$$309 \quad S(x) = \frac{1}{\exp[A(a - x)] + \exp[B(b - x)] + \exp[C(c - x)] + D'}$$

310 where $x = \lambda_{max}/\lambda$, $A = 69.7$, $a = 0.88$, $B = 28$, $b = 0.922$, $C = -14.9$, $c = 1.104$, and $D =$
 311 0.674 (3).

312

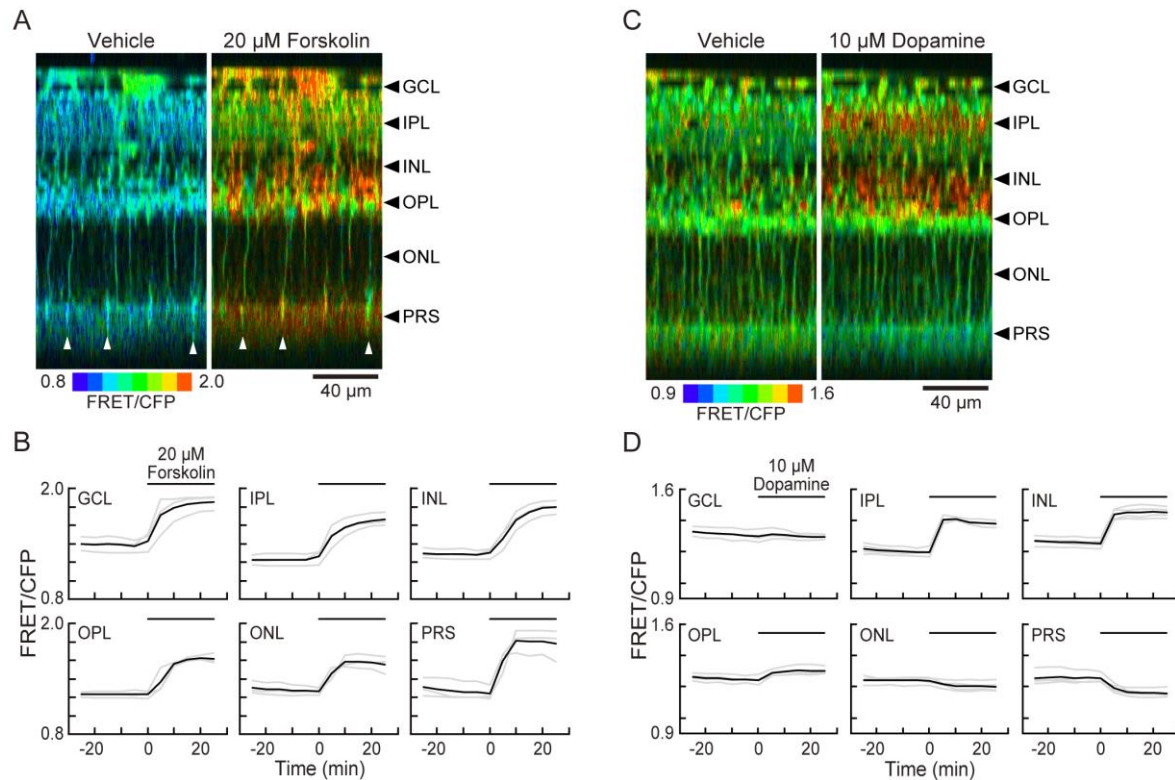
313

314 **Supplementary Figures**



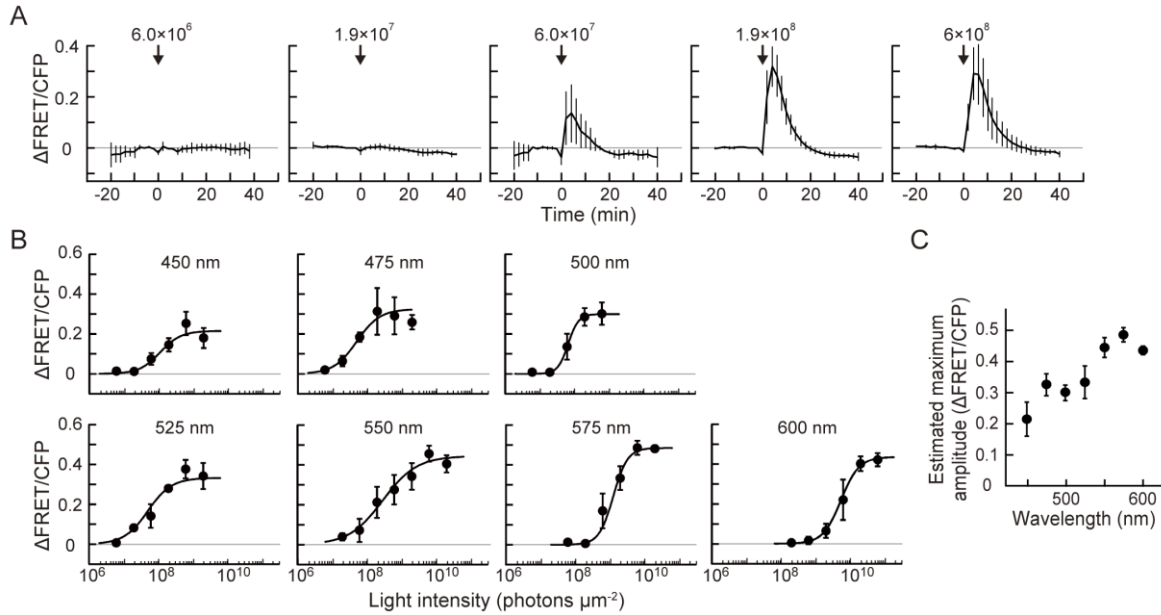
315 **Fig. S1.** Visualization of PKA activity using AKAR3EV FRET-biosensor.

316 (A) Predicted protein structure and mode of action of AKAR3EV. Activated PKA
317 phosphorylates the threonine residue in the PKA substrate motif. Phospho-threonine is
318 then recognized by the forkhead-associated (FHA) domain to promote FRET from cyan
319 fluorescent protein (CFP) to yellow fluorescent protein (YFP), which increases yellow
320 fluorescence. (B) Generation of a FRET/CFP ratio image to visualize PKA activity. The
321 fluorescent emission from the PKAchu retina is separated into yellow and cyan light and
322 received by two detectors, the FRET and CFP channels, respectively. The intensity of
323 each pixel in the FRET channel image is divided by that of the CFP channel image to
324 generate an 8-color FRET/CFP ratio image (see the *Supplementary Methods* for detail).
325 Sample images are obtained from light-stimulated photoreceptor cells (Fig. 3A). (C)
326 AKAR3EV-NC for the negative control. The PKA phosphorylation site, threonine, is
327 substituted to alanine so that FRET efficiency is not affected by PKA.
328

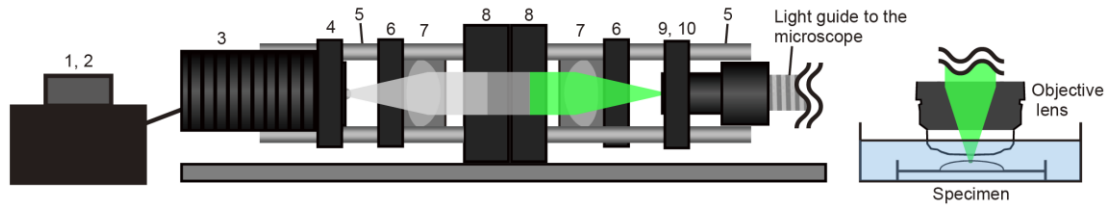


329 **Fig. S2.** Forskolin and dopamine responses in the PKAchu retina.

330 (A) Longitudinal images of the PKA activity before and after the perfusion of 20 μM
 331 forskolin. Images were reconstructed from a z-stack of 43 images with 4.5 μm -
 332 intervals. White arrowheads indicate cones. Black arrowheads indicate the positions of
 333 the layers analyzed in (B). (B) Time courses of forskolin-induced PKA activations at
 334 each layer. (C) Longitudinal images of the PKA activity before and after the perfusion of
 335 10 μM dopamine. Images were reconstructed from a z-stack of 40 images with 5 μm z-
 336 intervals. (D) Time courses of dopamine-induced PKA activity changes at each layer. For
 337 both (B) and (D), data points were obtained every 5 min and horizontal bars show the
 338 timing of drug perfusion. Light-colored and dark-colored curves are individual and
 339 averaged data, respectively. $n = 3$ and 4 for forskolin and dopamine, respectively.



340 **Fig. S3.** Intensity-response relationships of the light-off-induced PKA activation.
 341 (A) Rod responses toward 6 sec stimulation of various intensities of light at 500 nm.
 342 Numbers indicate the light intensity (photons μm⁻²) and arrows indicate the timing of the
 343 stimulation. Data were obtained every 2 min. Values are the mean ± SD (n = 3). (B)
 344 Intensity-response relationships of the light-off-induced PKA activation at each indicated
 345 wavelength. Values are the mean ± SEM (n = 3 to 7). (C) Relationship between the
 346 estimated maximum response amplitude and wavelength of the stimulation light. Values
 347 are the mean ± SEM (n = 3 to 7).



Components

Number	Component	Catalog number*	Quantity
1	Power supply	TPS001	1
2	LED driver	LEDD1B	1
3	White LED	MNWHL4	1
4	Cage plate	CP12	1
5	Cage assembly rods	ER3-P4	2
6	Cage plate	CP02/M	2
7	Lens	AC254-030-A-ML	2
8	Sliding filter mount	CFS1/M	2
9	Optic mount	CXY1	1
10	Adaptor	AD15F	1

*Thorlabs

Filters used in the component #8

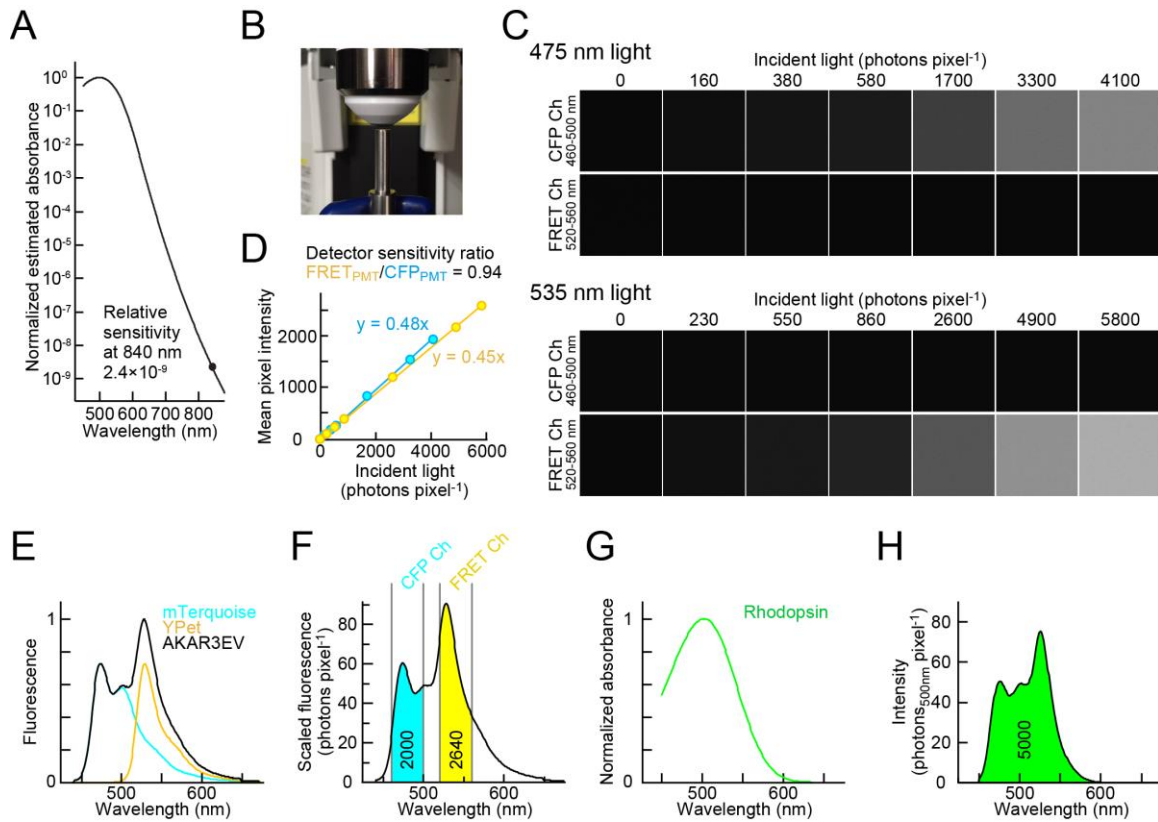
Product name	Catalog number*
400, 450, 500, 550, 600, 650 and 700 nm bandpass filter kit	#88-300
425 nm bandpass filter	#87-787
475 nm bandpass filter	#87-788
525 nm bandpass filter	#87-789
575 nm bandpass filter	#87-790
625 nm bandpass filter	#87-791
675 nm bandpass filter	#87-792
ND1 filter	#48-090
ND2 filter	#48-092
ND3 filter	#48-093
ND4 filter	#36-273

*Edmund optics

348 **Fig. S4.** Custom-made LED light stimulation system.

349 (A) Layout of the system. Numbers indicate the components listed below. Filters used in

350 component #8 are also listed.



351 **Fig. S5.** Estimation of the amount of photopigment activation during two-photon
 352 imaging.
 353 (A) The rhodopsin absorbance template extended to the infrared wavelength. (B) A
 354 picture of the photon injection setup. (C) Images obtained with CFP Ch and FRET Ch
 355 detectors when injecting indicated number of photons at 475 nm (upper panels) or 535
 356 nm (lower panels). (D) Relationships of incident light intensity and mean pixel intensity
 357 of images. (E) A predicted emission spectrum of AKAR3EV. (F) A scaled spectrum.
 358 Numbers show areas of colored regions. (G) The normalized absorbance spectrum of
 359 rhodopsin. (H) A spectrum obtained by multiplying (F) by (G). The number is the area of
 360 green region.
 361

362 **Legends for Supplementary Movies**

363

364 **Movie S1** (separate file) Z-stack images of the PKAchu retina. Two hundred cross-
365 sectional images were obtained in a 105 μm square area with 1 μm z-intervals.

366

367 **Movie S2** (separate file) Three-dimensional reconstruction of PNA-labeled
368 photoreceptors. PNA-labeled cone sheaths (magenta) and AKAR3EV^{high} cells (green)
369 were imaged.

370

371 **Movie S3** (separate file) Forskolin response of the PKAchu retina. Longitudinal images
372 were reconstructed from 43 cross-sectional images with 4.5 μm z-intervals. The time-
373 lapse interval was 5 min. Forskolin was continuously delivered from time 0.

374

375 **Movie S4** (separate file) Dopamine response of the PKAchu retina. Longitudinal images
376 were reconstructed from 40 cross-sectional images with 5 μm z-intervals. Dopamine was
377 continuously delivered from time 0.

378

379 **Movie S5** (separate file) The light-off-induced PKA activation after a 10 min-stimulation.
380 Data were obtained from a retinal explant prepared from the light-adapted PKAchu.
381 Images are cross-sectional views from the PRS layer. Light stimulation (500 nm, $3.2 \times$
382 10^7 photons μm^{-2} sec⁻¹) was given from -10 to 0 min. The time-lapse interval was 2 min.

383

384 **Movie S6** (separate file) Responses in PKAchu and PKAchu-NC retinal explants toward
385 6 sec-light stimulation. Images are cross-sectional views from the PRS layer. Stimulation
386 light (500 nm, 1.0×10^8 photons μm^{-2} sec⁻¹) was projected just before time 0 at the center
387 of the view field indicated as dashed circles. The time-lapse interval was 2 min.

388

389 **Movie S7** (separate file) Cell-type specificity of the light-off-induced PKA activation.

390 Longitudinal images were reconstructed from 35 cross-sectional images with 5 μm z-

391 intervals. Light stimulation (500 nm, 1.0×10^8 photons μm^{-2} sec $^{-1}$, 6 sec) was given.

392

393 **Movie S8** (separate file) High-magnification cross-sectional images of the light-off-

394 induced PKA activation at the PRS layer. Light stimulation (500 nm, 1.0×10^8 photons

395 μm^{-2} sec $^{-1}$, 6 sec) was given just before time 0. Note that bright spots are cones.

396

397 **Movie S9** (separate file) Comparison of the light-induced PKA activity changes between

398 wild-type and albino PKAchu photoreceptor cells. Images are cross-sectional views from

399 the PRS layer. Wild-type data are those used in Movie S5. Light stimulation (500 nm, 3.2

400 $\times 10^7$ photons μm^{-2} sec $^{-1}$) was given from -10 to 0 min.

401

402 **SI References**

403

404 1. T. Euler, K. Franke, T. Baden, "Studying a light sensor with light: multiphoton imaging in
405 the retina" in Multiphoton Microscopy, E. Hartveit, Ed. (Humana Press, 2019), vol. 148,
406 chap. 10, pp. 225-250.

407 2. G. Palczewska *et al.*, Human infrared vision is triggered by two-photon chromophore
408 isomerization. *Proc Natl Acad Sci U S A* **111**, E5445-5454 (2014).

409 3. V. I. Govardovskii, N. Fyhrquist, T. Reuter, D. G. Kuzmin, K. Donner, In search of the
410 visual pigment template. *Vis Neurosci* **17**, 509-528 (2000).

411 4. K. Sakurai *et al.*, Physiological properties of rod photoreceptor cells in green-sensitive
412 cone pigment knock-in mice. *J Gen Physiol* **130**, 21-40 (2007).

413 5. P. H. M. Bovee-Geurts, J. Lugtenburg, W. J. DeGrip, Coupled HOOP signature correlates
414 with quantum yield of isorhodopsin and analog pigments. *Biochim Biophys Acta*
415 *Bioenerg* **1858**, 118-125 (2017).

416 6. M. J. Mattapallil *et al.*, The Rd8 mutation of the Crb1 gene is present in vendor lines of
417 C57BL/6N mice and embryonic stem cells, and confounds ocular induced mutant
418 phenotypes. *Invest Ophthalmol Vis Sci* **53**, 2921-2927 (2012).

- 419 7. N. Le Fur, S. R. Kelsall, B. Mintz, Base substitution at different alternative splice donor
420 sites of the tyrosinase gene in murine albinism. *Genomics* **37**, 245-248 (1996).
- 421 8. P. D. Calvert *et al.*, Phototransduction in transgenic mice after targeted deletion of the rod
422 transducin alpha -subunit. *Proc Natl Acad Sci U S A* **97**, 13913-13918 (2000).
- 423 9. E. Ivanova, A. H. Toychiev, C. W. Yee, B. T. Sagdullaev, Optimized protocol for retinal
424 wholemount preparation for imaging and immunohistochemistry. *J Vis Exp*
425 10.3791/51018, e51018 (2013).
- 426 10. L. Bhatt, G. Groeger, K. McDermott, T. G. Cotter, Rod and cone photoreceptor cells
427 produce ROS in response to stress in a live retinal explant system. *Mol Vis* **16**, 283-293
428 (2010).
- 429 11. P. R. Williams, J. L. Morgan, D. Kerschensteiner, R. O. Wong, In vitro imaging of retinal
430 whole mounts. *Cold Spring Harb Protoc* **2013** (2013).
- 431 12. A. Parslow, A. Cardona, R. J. Bryson-Richardson, Sample drift correction following 4D
432 confocal time-lapse imaging. *J Vis Exp* 10.3791/51086 (2014).
- 433 13. J. N. Kapur, P. K. Sahoo, A. K. C. Wong, A new method for gray-level picture
434 thresholding using the entropy of the histogram. *Comput Vision Graph* **29**, 273-285
435 (1985).
- 436 14. H. Imai *et al.*, Molecular properties of rhodopsin and rod function. *J Biol Chem* **282**,
437 6677-6684 (2007).
- 438 15. T. Yoshizawa, G. Wald, Pre-lumirhodopsin and the bleaching of visual pigments. *Nature*
439 **197**, 1279-1286 (1963).
- 440 16. K. Sato *et al.*, Opn5L1 is a retinal receptor that behaves as a reverse and self-regenerating
441 photoreceptor. *Nat Commun* **9**, 1255 (2018).
- 442 17. J. Fan, B. Rohrer, G. Moiseyev, J. X. Ma, R. K. Crouch, Isorhodopsin rather than
443 rhodopsin mediates rod function in RPE65 knock-out mice. *Proc Natl Acad Sci U S A*
444 **100**, 13662-13667 (2003).
- 445